Atmos. Chem. Phys. Discuss., 14, 8575–8632, 2014
www.atmos-chem-phys-discuss.net/14/8575/2014/
doi:10.5194/acpd-14-8575-2014

Atmospheric Chemistry and Physics Discussions

Modeling global impacts of heterogeneous loss of HO_2 on cloud droplets, ice particles and aerosols

V. Huijnen[1], **J. E. Williams**[1], **and J. Flemming**[2]

[1]Royal Dutch Meteorological Institute, De Bilt, the Netherlands
[2]European Centre for Medium-Range Weather Forecasts (ECMWF), Reading, UK

Received: 10 February 2014 – Accepted: 18 March 2014 – Published: 31 March 2014

Correspondence to: V. Huijnen (huijnen@knmi.nl)

Published by Copernicus Publications on behalf of the European Geosciences Union.

Abstract

The abundance and spatial variability of the hydroperoxyl radical (HO_2) in the troposphere strongly affects atmospheric composition through tropospheric ozone production and associated HO_x chemistry. One of the largest uncertainties in the chemical HO_2 budget is its heterogeneous loss on the surface of cloud droplets, ice particles and aerosols. We quantify the importance of the heterogeneous HO_2 loss at global scale using the latest recommendations on the scavenging efficiency on various surfaces. For this we included the simultaneous loss on cloud droplets and ice particles as well as aerosol in the Composition-Integrated Forecast System (C-IFS). We show that cloud surface area density (SAD) is typically an order of magnitude larger than aerosol SAD, using assimilated satellite retrievals to constrain both meteorology and global aerosol distributions. Depending on the assumed uptake coefficients, loss on liquid water droplets and ice particles accounts for ~ 53–70 % of the total heterogeneous loss of HO_2, due to the ubiquitous presence of cloud droplets. This indicates that HO_2 uptake on cloud should be included in chemistry transport models that already include uptake on aerosol. Our simulations suggest that the zonal mean mixing ratios of HO_2 are reduced by ~ 25 % in the tropics and up to ~ 50 % elsewhere. The subsequent decrease in oxidative capacity leads to a global increase of the tropospheric carbon monoxide (CO) burden of up to 7 %, and an increase in the ozone tropospheric lifetime of ~ 6 %. This increase results in an improvement in the global distribution when compared against CO surface observations over the Northern Hemisphere, although it does not fully resolve the wintertime bias in the C-IFS. There is a simultaneous increase in the high bias in C-IFS for tropospheric CO over the Southern Hemisphere, which constrains on the assumptions regarding HO_2 uptake on a global scale. We show that enhanced HO_2 uptake on aerosol types associated with anthropogenic sources could contribute to reductions in the low bias for CO simulated over the extra-tropical Northern Hemisphere.

ACPD
14, 8575–8632, 2014

1 Introduction

Atmospheric lifetimes of gaseous pollutants and greenhouse gases are determined by their reactions with oxidants. The key tropospheric oxidants are the hydroxyl radical (OH), ozone (O_3) and, to a lesser extent, the nitrate radical (NO_3) and the halogen radicals. The resident mixing ratios of such oxidants are closely linked to the resident mixing ratios of the hydroperoxyl radical (HO_2) as the result of radical-radical interactions (Logan et al., 1981). One important route for HO_2 loss is the oxidation of nitric oxide (NO) to nitrogen dioxide (NO_2), which is crucial for the formation of tropospheric O_3. An alternative pathway for HO_2 loss is the uptake and/or scavenging by aerosol, ice and cloud particles (Liang and Jacob, 1997; Jacob, 2000). In the past, the impact of HO_2 uptake on heterogeneous surfaces has received less attention in laboratory and modelling studies than the uptake of N_2O_5, even though it has been shown to play a significant role in the troposphere (Tie et al., 2001; Martin et al., 2003; Liao and Seinfeld, 2005). More recently, global modeling studies using Chemistry Transport Models (CTMs) have shown that including heterogeneous loss of HO_2 on aerosol surfaces can have a significant effect on atmospheric composition by increasing the tropospheric burden of carbon monoxide (CO) and other trace gases as a result of a reduction in oxidative capacity (Macintyre and Evans, 2011; Lin et al., 2012; Mao et al., 2013).

While most previous modeling studies have focused on the uptake of HO_2 on aerosol surfaces, fewer studies considered HO_2 uptake on cloud and ice particles. This is despite the fact that the solubility of HO_2 is rather high, implying that uptake into cloud droplets under ambient tropospheric conditions could be significant (Thornton et al., 2008; Tilgner et al., 2005). Furthermore, the global surface area density (SAD) of cloud droplets is more than an order of magnitude larger than that of aerosol SAD, especially in regions away from strong aerosol sources such as over the Arctic, Atlantic/Pacific regions. The volume of tropospheric air occupied by liquid clouds is typically only a fraction of the total tropospheric volume (Jacob, 2000). The cloud fraction, as provided in the ECMWF meteorological analyses, reaches a value of $\sim 15\,\%$ as a global average

ACPD
14, 8575–8632, 2014

at ∼ 800 hPa altitude. Nevertheless, cloud chemistry of short-lived components can have a significant effect on tropospheric composition. Morita et al. (2004) have suggested that efficient HO_2 uptake by water surfaces takes place, based on molecular dynamics calculations. Once phase transfer has occurred HO_2 dissociates to H^+ and O_2^- depending on the pH of the droplet, with the characteristic pKa value being 4.8 (Bielski et al., 1985). By the efficient scavenging of soluble precursors, such as hydrogen peroxide (H_2O_2) and formaldehyde (HCHO), aqueous phase chemistry plays a significant role in the global HO_x budget (Lelieveld and Crutzen, 1991; Ervens et al., 2003). For example, in complex 1-D column model studies Williams et al. (2002) have shown that strong reductions of between ∼ 30–40 % in HO_x mixing ratios occur during cloud events as a consequence of HO_2 uptake on clouds and aquated aerosol over the polluted marine boundary layer. Such reductions have also been confirmed during in-flight observations of HO_x radicals above West Africa (Commane et al., 2010).

The rates of heterogeneous uptake reactions are generally modeled using a first-order loss rate depending on a characteristic uptake coefficient (γ), (Schwartz, 1986), which describes the likelihood that uptake will occur when a collision happens between the gas-phase molecule and the surface. $\gamma(HO_2)$ values between 2×10^{-3} and 1.0 have been reported in the literature based on laboratory, field, and modelling studies (Mozurkewich et al., 1987; Cooper and Abbatt, 1996; Thornton and Abbatt, 2005; Bedjanian et al., 2005; Thornton et al., 2008; Loukhovitskaya et al., 2009; Whalley et al., 2010; Taketani et al., 2012; Mao et al., 2013; Liang et al., 2013). HO_2 heterogeneous reaction on aerosol is thought to be an important process required to explain observations of atmospheric composition over the Arctic (Mao et al., 2010; Olsson et al., 2012). Studies of heterogeneous reactions on aerosol surfaces have highlighted the sensitivity to pH, the aerosol hygroscopic properties and the availability of Transition Metal Ions (TMI), namely iron and copper ions. Also several reaction pathways leading to different product distributions have been proposed (Jacob et al., 2000; De Reus et al., 2005; Mao et al., 2013; Liang et al., 2013), although they have yet to be supported by corresponding laboratory measurements.

ACPD
14, 8575–8632, 2014

Modeling the global impact of heterogeneous HO_2 uptake requires an accurate description of the available SAD integrated for the different types of aerosol and cloud particles. Also the hygroscopy of the aerosol has to be known as the acidity in the droplet is important for the speciation of TMI in the solution (e.g. Ervens et al., 2003).

For example, colloidal speciation of TMI has been found in measurements of chemically aged rainwater (Parazois et al., 2006) showing that a large fraction of TMI are not simply in the aquated form.

At present there is a wide variety of global CTMs which simulate aerosols together with gas-phase chemistry (Myhre et al., 2013), with a wide range of simulated interactions. Tropospheric aerosol impacts on gas-phase chemistry via heterogeneous reactions as well as the perturbations of photolysis rates by enhanced scattering and absorption. For instance, the GEOS-Chem and MOZART CTMs apply a bulk aerosol model (e.g. Tie et al., 2005; Thornton et al., 2008; Mao et al., 2013), while ECHAM-HAM and TM5 apply a modal scheme, where the aerosol particle size distribution is described by 7 lognormal modes (Vignati et al., 2004; Pozzoli et al., 2008; Aan den Brugh et al., 2011). Our study uses the weather forecast model with online integrated aerosol and chemistry modules (Flemming et al., 2014) of the European Centre for Medium range Weather Forecasting (ECMWF), which is referred to as "Composition-Integrated Forecast System" (hereafter C-IFS). C-IFS applies the modified CB05 chemistry mechanism (Williams et al., 2013) and a bulk aerosol scheme (Morcrette et al., 2009), which has been extended to include nitrate (NO_3^-) and ammonium (NH_4^+) aerosol available from the gas-phase chemistry scheme. The meteorological model used in C-IFS is initialized by operational daily ECMWF meteorological analyses. Clouds are described by the use of prognostic variables for cloud liquid water, cloud ice and cloud fraction (IFS documentation Cy38r1, 2013).

In this paper we assess the impact of accounting for the heterogeneous uptake of HO_2 by tropospheric aerosol, cloud droplets and ice particles on the tropospheric gas phase chemistry represented by the chemical ozone budget and the oxidation capacity. We use HO_2 scavenging coefficients which are taken from the latest recommendations.

ACPD
14, 8575–8632, 2014

The aerosol concentrations used in our study are taken from the MACC re-analysis (Morcrette et al., 2011), which is constructed from the assimilation of aerosol optical depth (AOD) satellite observations (Benedetti et al., 2009). By having tropospheric chemistry implemented in the meteorological model we can fully exploit the availability of meteorological parameters applied in physics parameterizations (Flemming et al., 2014).

This paper is structured as follows. In Sect. 2, we give an overview of the modeling system, discuss the uptake coefficients provided in the literature and provide details of the model sensitivity experiments. In Sect. 3 we evaluate the performance of the C-IFS by comparing against a variety of measurements and provide a discussion of the results. Here we also present the effects of various assumptions on global composition. In Sect. 4 we provide further discussion of the uncertainties related to our approach, and finally, in Sect. 5, we summarize our conclusions.

2 Model overview

The IFS of the European Center for medium Range Weather Forecasts has recently been extended to include both aerosols (Morcrette et al., 2009) and chemistry (Flemming et al., 2014) within the framework of the MACC project (Monitoring Atmospheric Composition and Climate, www.copernicus-atmosphere.eu). The meteorological model in the current version of C-IFS is based on IFS cycle 38r1 (http://www.ecmwf.int/research/ifsdocs/). This cycle benefits from the use of the updated microphysics scheme (Forbes et al., 2011), which includes the description of five prognostic variables (cloud fraction, cloud liquid water, cloud ice, rain and snow). We run the model at a spectral resolution of T159 ($\sim 1.125^{\circ}$) and with 60 hybrid sigma model levels.

The aerosol module describes the aerosol composition based on 5 different aerosol types, namely sea salt (SS), dessert dust (DD), sulphate (SO_4^{2-}), Black Carbon (BC) and Organic Matter (OM) (Morcrette et al., 2009). For sea salt and dust three size

ACPD
14, 8575–8632, 2014

bins are assumed, whereas for black carbon and organic carbon we differentiate between hydrophobic and hydrophilic aerosol types. Table 1 contains the density of each aerosol type and the assumptions regarding the effective radii to account for hygroscopic growth at increased relative humidity, required for the computation of the aerosol SAD. Hygroscopic growth with ambient moisture for different hydrophilic aerosol types is parameterized with the relative humidity (RH) prescribed by the ECMWF meteorological data following Chin et al. (2002). In our model simulations total aerosol is constrained by the data assimilation of observations from the Moderate Resolution Imaging Spectroradiometer (MODIS) TERRA and AQUA instruments (Remer et al., 2005). In the assimilation procedure the a priori model aerosol concentrations are scaled to optimize the total modeled AOD to the observations (Benedetti et al., 2009). Huijnen et al. (2012) showed that modeled a priori aerosol type, including assumed aerosol emissions, is crucial to achieve a successful constraint on aerosol speciation.

The tropospheric chemistry in the C-IFS is described by the recently developed modified CB05 scheme (Williams et al., 2013). This is a reduced version of the CB05 chemical mechanism (Yarwood et al., 2005), where selected reactions and product distributions are taken from Zaveri and Peters (1999). Acetone (CH_3COCH_3) chemistry was also added. Compared to the work presented in Williams et al. (2013) in our study the mechanism was modified as follows: (i) the product yield for the self reaction of methylperoxy radical was updated following Yarwood et al. (2005), (ii) two explicit tracers were added for the higher C3 peroxy-radicals formed during the oxidation of C_3H_6 and C_3H_8, respectively, following Emmons et al. (2010) to introduce a term for the chemical production of CH_3COCH_3 and the higher aldehydes and (iii) the yield of methacrolein and methyl-vinyl ketone (lumped as ISPD) from isoprene oxidation was decreased as motivated by an intercomparison between chemical mechanisms (Archibald et al., 2010). These updates are summarized in Table 2. Both NO_3^- and NH_4^+ aerosol components are not part of the MACC aerosol model (Morcrette et al., 2009) but their formation rates are based on the EQSAM solver (Metzger et al., 2001) as taken over from the TM5 chemistry transport model (Huijnen et al., 2010). The same holds for the Euler

ACPD
14, 8575–8632, 2014

backward iterative chemical solver (Hertel et al., 1993). The modified band approach, which is adopted for the computation of photolysis rates (Williams et al., 2012), uses the actual aerosol absorption and scattering optical depths for each individual atmospheric column.

The parameterizations used for wet scavenging and dry deposition are described in Flemming et al. (2014) for the gas-phase species, and in Morcrette et al. (2009) for the aerosol species. The monthly mean dry deposition velocities are based on climatological fields taken from the MOCAGE CTM (Michou et al., 2004), except for CO, where a scaling based on soil wetness was applied (Sanderson et al., 2003; Stein et al., 2014). Stratospheric O_3 concentrations are constrained by the ECMWF operational analyses of O_3, hence ensuring realistic overhead columns and stratospheric ozone inflow. Surface methane concentrations are prescribed by a zonal, monthly climatology derived from flask observations at the surface from selected background stations situated in pristine regions near the dateline.

The anthropogenic emission estimates are based on the MACCity inventory (Granier et al., 2011). For biogenic emissions we adopt the POET database for 2000 (Granier et al., 2005; Olivier et al., 2003), with isoprene emissions being taken from MEGAN2.1 and valid for the year 2000 (Guenther et al., 2006). For biomass burning emissions we apply actual daily estimates taken from the Global Fire Assimilation System (GFAS) version 1 (Kaiser et al., 2012). The individual emission totals are provided in Table 3. Finally, Lightning NO_x emissions are calculated according to the parameterization of Meijer et al. (2001) which are dependent on the convective precipitation and scaled to give an annual total of $\sim 5\,\mathrm{Tg\,N\,yr^{-1}}$. For aircraft NO_x emissions $\sim 0.7\,\mathrm{Tg\,N\,yr^{-1}}$ are assumed (Lamarque et al., 2010). Aerosol emissions are as described in Morcrette et al. (2009) with aerosol fire emissions also derived from GFASv1 (Kaiser et al., 2012).

ACPD
14, 8575–8632, 2014

2.1 Heterogeneous uptake on surfaces

Heterogeneous reactions on aerosol and cloud particles are described by a pseudo first-order rate constant k_{het} using the theory of Schwartz (1986):

$$k_{het} = \left(\frac{r_e}{D_g} + \frac{4}{c\gamma} \right)^{-1} A \quad (1)$$

where r_e (cm) is the particle effective radius, D_g ($cm^2 s^{-1}$) is the gas phase diffusion coefficient, γ is the uptake coefficient, c ($cm s^{-1}$) is the mean molecular speed, and A is the cloud or aerosol surface area density ($cm^2 cm^{-3}$). The SAD for liquid cloud and aerosol particles is computed as:

$$A = \frac{3M}{\rho r_e} \quad (2)$$

with M being the particle mass density in the ambient air ($g cm^{-3}$) and ρ ($g cm^{-3}$) the density of the particle. Here we assume the shape of the particles to be spherical. For liquid and ice cloud SAD we scale M by the cloud fraction to obtain the SAD representative for the cloudy part of the grid cell. The effective cloud particle radius ($r_{e,\,cloud}$) is computed by the rather simple empirical relationship of Fouquart et al. (1990):

$$r_{e,\,cloud} = 4 + 11LWP \quad (3)$$

With LWP being the liquid water path ($g\ m^{-2}$), integrated per grid cell from the cloud liquid water content and scaled by the cloud fraction, and $r_{e,\,cloud}$ given in units (µm). For the computation of ice cloud SAD we apply the parameterization developed by Heymsfield and McFarquhar (1996):

$$A_{ice} = 10^{-4} IWC^{0.9} \quad (4)$$

ACPD
14, 8575–8632, 2014

Compared to observations, Popp et al. (2004) found that A_{ice} is too low, therefore Schmitt and Heymsfield (2005) suggested a multiplication by a factor 10 to account for irregularities in the ice particles. The effective ice particle radius $r_{e,\,ice}$ are computed according to the parameterization of Fu (1996):

$$r_{e,\,ice} = \frac{\sqrt{3}}{3\rho_{ice}} \frac{IWC}{A} \tag{5}$$

The heterogeneous reactions of N_2O_5 on cloud and aerosol surfaces which forms nitric acid (HNO_3) are included in all simulations (see Table 4). In addition, NO_3 loss on aerosol is assumed to take place with $\gamma(NO_3) = 10^{-3}$ following Jacob (2000).

Kolb et al. (2010) and Abbatt et al. (2012) have recently reviewed the current knowledge of $\gamma(HO_2)$ values in the absence of TMI. They note divergent recommendations for the uptake co-efficients. Furthermore, Abbatt et al. (2012) point out that the reactive uptake of HO_2 at room temperature is rather slow suggesting a small value of $\gamma(HO_2) < 0.01$ (Mozurkewich et al., 1987; Thornton and Abbatt, 2005). As pointed out by Thornton et al. (2008) this can be explained by the temperature dependent solubility of HO_2, which may still lead to values $\gamma(HO_2) > 0.1$ for weakly acidic, cold particles (i.e. pH 5, < 270 K), which are ubiquitous in the upper troposphere and in polar regions. In contrast, Taketani et al. (2008) measured efficient first order loss of HO_2 over a range of aqueous inorganic particles at room temperature, suggesting a higher $\gamma(HO_2)$ of ~ 0.1, with the loss being generally enhanced at higher relative humidity levels. Moreover, $\gamma(HO_2)$ becomes > 0.05 for RH > 50 % on hygroscopic salts and on water-soluble organic aerosol due to enhanced solubility. Earlier studies that use macroscopic films of cold liquid water and/or sulfuric acid solutions find generally a $\gamma(HO_2) > 0.05$ (e.g., Cooper and Abbatt, 1996). Thus Abbatt et al. (2012) conclude that further validation experiments are required to reconcile the conflicting vales of results of $\gamma(HO_2)$, such as those recently performed by George et al. (2013), where $\gamma(HO_2) < 0.02$ was measured on aqueous inorganic salt aerosols.

ACPD
14, 8575–8632, 2014

The presence of transition metal ions (TMI) in aerosol particles is thought to strongly enhance HO_2 uptake by introducing the direct reduction of aquated HO_2 radicals, as shown in the box modeling studies of Tilgner et al. (2005). TMI are considered ubiquitous in aerosol particles (Mao et al., 2013), especially in the vicinity of anthropogenic sources. For instance, local measurements of $\gamma(HO_2)$ on aerosol particles in and nearby Beijing, China have shown values up to 0.4 (Taketani et al., 2012) and 0.86 (Liang et al., 2013), respectively, hence it has been postulated that TMI play a significant role in polluted areas. Nevertheless, little quantitative information is available in the literature on the size-resolved concentrations of TMI in ambient aerosol particles to make assessments in this regard.

In their mechanism Mao et al. (2013) suggest that no H_2O_2 is formed during the loss of HO_2 on aerosol surfaces, which has previously been invoked in order to explain the observational evidence of low H_2O_2 in presence of aerosol concentrations (e.g., Mao et al., 2010; De Reus et al., 2005). However, H_2O_2 is also thought to be formed within cloud droplets and aquated aerosols by photochemical radical chemistry thus reducing the uptake (Anastasio et al., 1994; Arakaki et al., 1995; Wang et al., 2010) although this is thought to be a secondary source compared to the direct phase transfer from the gas phase (Marinoni et al., 2011). It has also been postulated that the de-gassing of dissolved compounds during the evaporation of cloud droplets could be a source of gas-phase H_2O_2 under certain conditions (Zuo and Hoigne, 1992).

Considering that no consensus has been reached regarding the most relevant value for $\gamma(HO_2)$ on aerosol particles we choose to select a lower limit as discussed in Abbatt et al. (2012) (see Table 5) in order not to overestimate the effect. However, we carried out an additional sensitivity simulation where $\gamma(HO_2)$ is set to 0.7 on aerosol types that are mostly associated to anthropogenic origin (SO_4^{2-}, NO_3^-, BC), i.e. for those aerosols for which high values for $\gamma(HO_2)$ have been observed (Liang et al., 2013; Taketani et al., 2012). This provides an estimate of the impact on atmospheric composition when assuming a relatively large efficiency of HO_2 uptake on aerosol.

ACPD
14, 8575–8632, 2014

Only few publications report on the actual uptake efficiency of HO_2 on clouds, despite its importance (e.g., Jacob et al., 2000; Tilgner et al., 2005). Here we assume $\gamma(HO_2)$ on liquid cloud to be 0.06, which is lower than the value suggested for salt solutions (Kolb et al., 2010), and the value implied by Morita et al. (2004) of 0.2, so should be considered as a lower limit. Once scavenged into solution HO_2 undergoes dissociation (pKa $\sim$ 4.8, Bielski et al., 1985) where the pH of cloud droplets can range from 4 (polluted) to 7 (remote) therefore phase equilibrium is rarely achieved. For the uptake of HO_2 on ice particles we follow the IUPAC recommendation based on Cooper and Abbatt (1996). Considering the limited area of the grid cell where clouds are present, an assumption has to be made on the subgrid-scale processing (Liang and Jacob, 1997). Based on an assessment of the HO_2 chemical budget under cloudy conditions, we find that the HO_2 heterogeneous loss is relevant, but not the dominating term in the overall chemistry budget. This will also be illustrated by the global HO_2 budget presented in Sect. 3.4. Therefore the assumption of subgrid-scale mixing between cloudy and cloud-free parts of the grid cell after every time step will not lead to an over-estimation of the HO_2 loss through the cloudy part of the grid cell: other chemistry terms are still dominating the sub-grid HO_2 budget. Therefore we scale k_{het} by the cloud fraction, to obtain a grid-cell average reaction rate.

In our study we assume that no HO_2 or H_2O_2 is released from the cloud or aerosol particles during evaporation, but by choosing the lower limit for $\gamma(HO_2)$ on aerosol, and cloud droplets, we in some way account for the in-situ formation of H_2O_2 in aerosol particles, which is thought to occur when accounting for the detailed aqueous phase chemistry. In Sect. 4 we review the uncertainties related to the heterogeneous uptake parameterization in our simulations.

2.2 Definition of the sensitivity studies and emission estimates

We have performed four different sensitivity experiments with C-IFS using $\gamma(HO_2)$ values provided in Table 5. These comprise of (i) a simulation with no heterogeneous uptake of HO_2 (BASE) (ii) a simulation where HO_2 uptake on aerosol is included using

ACPD
14, 8575–8632, 2014

a constant value for $\gamma(HO_2) = 0.06$ following Abbatt et al. (2012) (AER), (iii) a simulation as AER but with uptake on cloud and ice particles additionally included (AER-CLD) and (iv) a simulation as AER-CLD except that a $\gamma(HO_2) = 0.7$ is applied on a limited set of aerosol types (SO_4^{2-}, NO_3^- and BC), as motivated by recent field measurements in urban environments (Taketani et al., 2012; Liang et al., 2013), run AER-S-CLD.

By initializing meteorology and aerosol concentrations on a daily basis this provides constraints on their respective uncertainties, and hence on the associated cloud and aerosol SAD.

2.3 Observational datasets

For the validation of the distribution of selected trace gas species in the C-IFS and the quantification of the effects on these species, we use in-flight observations from the DC-8 aircraft over the Arctic, taken during April and between June–July in 2008 as part of the Arctic Research of the Composition of the Troposphere from Aircraft and Satellites (ARCTAS) campaign (Jacob et al., 2010). The availability of observations of a host of different trace gases, including HO_2, enables a critical assessment of the performance of the C-IFS over the (remote) Arctic region during both the Arctic spring and summer. While the springtime flights were designed to study mainly the impact of mid-latitude pollution to the Arctic, the summertime flights were focusing on radical photochemistry, the quantification of boreal fire emissions, and their impacts on ozone production (Jacob et al., 2010). In our analysis we use the observations north of 45° N, where the flight routes are shown in Fig. 1. Uncertainties in the measurement of trace gas mixing ratios were reported to be of the order of 3 % for O_3, 12 % ± 26 pptv for CH_2O and 32 % for HO_2 and 50 % ± 100 pptv for H_2O_2 (Olson et al., 2012).

Tropospheric O_3 profiles are further evaluated using a selection of composites assembled using data taken from the World Ozone and Ultraviolet Radiation Data Centre (WOUDC) balloon sonde data. The selected sites are Tateno (140.1° E, 36.1° N), Hohenpeissenberg (11.0° E, 47.8° N), Nairobi (36.8° E, 1.3° S) and Neumayer (8.3° W, 70.7° S), which provide coverage for both the tropics and extra-tropics. We evaluate

ACPD
14, 8575–8632, 2014

surface carbon monoxide mixing ratios against NOAA Earth System Research Laboratory (ESRL) Global Monitoring Division (GMD) observations at selected background stations. Here we use data from the stations Alert (62° W, 82° N), Mace Head (10° W, 53° N), Tenerife (16° W, 28° N), Assekrem (5° E, 23° N), Ascension Island (14° W, 8° S), Mauna Loa (155° W, 19° N), Samoa (170° W, 14° S) and Syowa (39° E, 69° S). Furthermore, CO total columns are compared against the day-time data from the multispectral thermal infrared (TIR)/near infrared (NIR) MOPITT-V6 product (Deeter et al., 2012, 2013), where we apply the averaging kernel to the model profiles, and additionally average pixels binned within 1° × 1° within each month.

3 Results

In this section we first provide a summary of the performance of the aerosol fields from the literature. This is followed by a general overview of the global distribution of cloud and aerosol SAD and its impact on HO_2 as modelled in our study. We compare co-located tracer distributions against ARCTAS data for April/June–July 2008, which provides constraints on HO_2, and other chemical compounds over the remote Arctic region. Last we evaluate tropospheric O_3 and CO on a global scale with respect to the different approaches to the modelling of heterogeneous HO_2 uptake.

3.1 The aerosol fields

In our study aerosol fields are strongly constrained by the MACC reanalysis (Morcrette et al., 2011), which have been extensively validated (Eskes et al., 2013; Bellouin et al., 2013). The validation against independent Aeronet data of AOD (Dubovik et al., 2002) has shown that European total AOD exhibits a small, homogeneous positive bias of ∼ 10 %. For the Sahel zone, the total AOD is underestimated by ∼ 10 %, caused by a low bias in largest dust particles, despite a positive bias for the smallest dust particles. Also a low bias in the biomass burning aerosol is found (Eskes et al., 2013). For North

ACPD
14, 8575–8632, 2014

America a high bias of ∼ 40–60 % exists, although this is somewhat smaller over the more polluted Eastern part of North America. The total AOD at remote oceanic sites in the southern oceans is also considerably overestimated (+100 %) suggesting an over-estimate of sea salt contributions. Variable small biases of within 20 % are seen in Eastern Asia. Overall, the correlation between the MACC reanalysis and the Aeronet data for AOD for the year 2008 is good (r = 0.87), with a (positive) normalized mean bias of 15.1 % based on daily data. Assuming an approximately linear relationship between aerosol density and SAD (see Eq. 2), this suggests a corresponding global over-estimation of aerosol SAD in the same order of magnitude.

3.2 SAD and its impact on HO_2

Figures 2 and 3 present the zonal and horizontal mean distributions of the monthly mean SAD, respectively, for April 2008. At 800 hPa it can be seen that liquid cloud SAD dominates the total SAD, with values generally being an order of magnitude larger than those from both ice cloud and aerosol, except for over the (dry) desert regions. The maximum liquid cloud SAD values can be found near the storm tracks in the Southern Hemisphere (SH). The zonal mean projection shows that levels of ice cloud SAD are significant at high latitudes (> 70° S/° N) and up in the upper tropical troposphere between 150–400 hPa, where cold temperatures persist. The zonal distributions of cloud and aerosol SAD shows that in the tropics (30° S–30° N), where a large fraction of global oxidation occurs due to high water vapour and high temperatures, the SAD from cloud droplets dominates. While liquid cloud SAD maximizes at an altitude of ∼ 850 hPa, aerosol SAD is increases towards the surface, especially over the major aerosol source regions in the Northern Hemisphere (NH).

Relatively high aerosol SAD is also found over the oceans in the SH, related to high sea salt concentrations. This contribution to the total aerosol SAD is most likely overestimated (see discussion in Sect. 4). Over the Arctic, where the majority of ARCTAS flights take place, the aerosol SAD at 800 hPa ranges between 40 and 100 $\mu m^{-2}\,cm^3$,

ACPD
14, 8575–8632, 2014

which appears about a factor 4 larger than found in the analysis by Olson et al. (2012), who assume dry aerosol particles.

The resulting effect on resident HO_2 mixing ratios when comparing BASE, AER and AER-CLD is shown in Fig. 4, where both the horizontal and zonal mean change in HO_2 mixing ratios are given. It can be seen that the HO_2 mixing ratios are highest within the tropics. Therefore, and because of the much larger area, the uptake on cloud droplets within the tropics dominates the global budget term for HO_2 loss by heterogeneous scavenging, when assuming a similar uptake efficiency for both cloud and aerosol.

Nevertheless, largest relative changes are found outside the tropics, as within the tropics the gas-phase photochemistry, characterized by fast photolysis rates, is dominating the HO_x budget at the expense of the heterogeneous loss. At the northern and southern mid-latitudes, where instances of full cloud coverage are frequent (see Fig. 3), and over regions with a strong contribution due to aerosol particles, the decrease in HO_2 mixing ratios are significant (> 30 %). For regions over the Arctic, the change shows a considerable variation with altitude with the strongest reductions being at altitudes between 1000 hPa and 800 hPa and around 400 hPa, likely related to the largest transport routes towards the Arctic. From these figures the relative importance of HO_2 uptake on cloud as compared to its uptake on aerosol becomes apparent.

For AER-S-CLD, which has enhanced scavenging efficiency on SO_4^{2-}, NO_3^- and BC aerosol, an additional reduction in HO_2 concentrations of 10–20 % on average is found over the extratropical NH as shown in Fig. 5. This figure indicates the largest decrease in HO_2 concentrations (up to 50 %) over the East-Asian source region and its outflow, where aerosol concentrations from anthropogenic origin exhibit high values.

A quantitative evaluation of changes in the tropospheric composition and the associated chemistry budgets is provided in the next subsections.

3.3 Evaluation of trace gas distributions against ARCTAS data

We evaluate the model results against in-flight observations taken as part of the ARCTAS aircraft campaign during both April and June–July 2008 (Sect. 2.3, Jacob et al.,

ACPD
14, 8575–8632, 2014

2010). The photochemistry at these high latitudes shows a strong seasonal cycle, with low activity in Arctic wintertime conditions. Moreover, the flux of photolysing radiation is further enhanced by the high albedo from persistent snow and sea ice surfaces.

Comparisons of the spring and summertime median vertical profiles for CO, O_3, HO_2, CH_2O and H_2O_2 are shown in Fig. 6. There is a general underestimation of tropospheric CO throughout the troposphere in April, similar to the findings by Shindell et al. (2006) for different global CTMs. This underestimation is less pronounced during the boreal summer, when photochemistry is active throughout the day. During April, AER-S-CLD shows the best agreement with the observations. With little local emissions, the distribution of CO in the Arctic is sensitive to the transport of both CO and its precursors into the region (Thomas et al., 2013; Stein et al., 2014). However, even with the application of relatively high-resolution transport and meteorology, C-IFS still leads to an under prediction in CO, suggesting missing CO and precursor emissions. The corresponding changes introduced for tropospheric O_3 are small due to the low photolysis frequency for NO_2 dampening the importance of the NO and HO_2 recycling reaction in terms of O_3 regeneration. Thus, the increases in CO occur due to the variability in oxidative capacity introduced outside the Arctic.

The observed tropospheric HO_2 mixing ratios during April are about a factor 3 lower than those in June, due to differences in the seasonal photochemical activity and the very short tropospheric lifetime. During April, BASE shows a good agreement when compared against the measured HO_2 mixing ratios while introducing heterogeneous loss results in an underestimation up to $\sim 30\,\%$. There is an associated underestimation of both OH and H_2O_2 by $\sim 50\,\%$ in both BASE and AER-S-CLD. Nevertheless, HO_2 from BASE showing the best agreement to observations is fortuitous as the H_2O_2 and CH_2O vertical profiles, both acting as dominant chemical precursors for HO_2 (Mao et al., 2010; Olson et al., 2012), are significantly underestimated. Therefore, the low HO_x in the C-IFS for April is most likely related to the uncertainties related to both transport into the region and the loss of H_2O_2 and CH_2O by wet scavenging. Evaluation of the vertical distribution of the most important chemical precursors of CH_2O,

ACPD
14, 8575–8632, 2014

such as CH_3CHO, C_3H_6, and C_3H_8 in C-IFS (not shown) against the corresponding ARCTAS data also shows a significant under-estimation in April. This suggests that transport of CH_2O and its precursors into the region from e.g. Northern Europe is too low (e.g., Williams et al., 2013). On the other hand, Olson et al. (2012) also showed that constraining H_2O_2 mixing ratios by using observations results in a significant over-estimation in HO_2 mixing ratios. To resolve this HO_2 uptake on aerosol was included using values from Thornton et al. (2008), although failed to fully resolve this positive bias.

In summary, the springtime evaluation does not prove conclusive with respect to the impact of the heterogeneous uptake of HO_2, with AER-S-CLD still showing an under-estimate in CO. This suggests that it is unlikely that a missing sink term for HO_2 is the main reason of the NH low bias in CO which occurs at these high northern latitudes, but rather missing chemical precursors either directly emitted or transported in the region.

Figure 6 shows that for the summer months of June and July there is a relatively good agreement in the tropospheric distribution in all trace species shown, with biases generally below 10 %, with the exception of H_2O_2. Given that photochemical production governs HO_2, shows that the modified band approach (Williams et al., 2006) as applied in C-IFS is able to model Arctic photochemistry rather well. Biases in the lower troposphere are linked to fresh fire plumes (Hornbrook et al., 2011), which reflect uncertainties in the assumed fire emissions from GFAS. The differences between the various runs for O_3 and CH_2O are rather negligible while for HO_2 (and OH, not shown) the three model runs show differences within the ~ 30 % uncertainty range associated with the measurements. CO concentrations increase by up to ~ 6 % in run AER-S-CLD compared to BASE, improving against the observations at altitudes above 700 hPa that are less affected by local emission sources.

Analysing the HO_2 comparison more closely shows that there is a decrease of ~ 10 % in the model around 900 hPa which is directly related to loss on aerosol surfaces (c.f. BASE and AER). This is further enhanced by an additional ~ 20 % when introducing additional loss on ice particles. At higher altitudes (~ 700 hPa) uptake on

ACPD
14, 8575–8632, 2014

ice particles (c.f. AER-CLD vs. AER) dominates, resulting in a sink term as efficient as on aerosol surfaces. Comparing AER-S-CLD vs. AER-CLD shows a maximal effect at ∼ 900 hPa, confirming that loss on tropospheric aerosol is most important for the boundary layer at such high latitudes. There still exists a significant underestimation in the modeled HO_2 profile especially in the boundary layer, most likely related to uncertainties in the modeling of fresh fire plumes.

For CH_2O in the lower atmosphere during summertime, C-IFS captures the correct vertical distribution in the free troposphere, showing that transport of air from other regions is modeled rather well. This is in sharp contrast to what was shown for April, and may point to the fact that there are strong seasonal cycles in precursor emissions related to biogenic activity (Williams et al., 2013) which would partly explain seasonal differences.

Again, these comparisons prove inconclusive towards which of the assumptions related to heterogeneous HO_2 uptake are the most plausible, but they show that for the current model setup a larger degree of heterogeneous uptake is not needed to match observed HO_x distributions in the Arctic. In the current evaluation this would actually lead to a degradation of the model performance, especially in AER-S-CLD. It should be noted that the photochemistry in the Arctic is challenging and may not be representative on a global scale, due to its particular meteorological circumstances and its relatively small areal contribution to the global chemistry budget.

3.4 Evaluation of tropospheric ozone

Table 6 provides an assessment of the tropospheric O_3 budget for the year 2008 as calculated in C-IFS for all four simulations. The associated zonal loss of HO_2 by heterogeneous uptake on aerosol and cloud surfaces vs. a selection of homogeneous loss terms in the gas-phase is presented in Table 7. For these global chemical budgets terms the tropopause is defined as the annual, zonal mean altitude where the mixing ratio of O_3 is less than150 ppb (Stevenson et al., 2006). Uncertainties in the global chemistry budget terms due to the definition of the tropopause are assumed to

ACPD
14, 8575–8632, 2014

be small, i.e. of the order of $\sim 20\,\mathrm{Tg\,yr^{-1}}$, based on offline budget computations of TM5 (Huijnen et al., 2010).

Accounting for a constant, but relatively small loss of HO_2 on cloud and aerosol surfaces (run AER-CLD vs. BASE) results in a decrease in the tropospheric O_3 production term by $179\,\mathrm{Tg\,O_3\,yr^{-1}}$ ($\sim 4.2\,\%$), which is directly related to the decrease in NO_2 regeneration through the oxidation of NO by HO_2. The increased uptake efficiency in AER-S-CLD enhances the net decrease in O_3 production by $\sim 6.2\,\%$ compared to BASE. The effects of the lower production terms on the tropospheric burden of O_3 are mitigated by a simultaneous reduction in the total amount of O_3 lost by reaction with both OH and HO_2, resulting in only a marginal net increase in the total tropospheric O_3 burden. There is an associated increase in the tropospheric lifetime of O_3 of up to $\sim 6\,\%$ in run AER-S-CLD (see Table 6). These modest changes imply that, at global scale, the average differences in O_3 are rather small, although locally differences can be larger, as discussed below.

When integrated over the entire year the subsequent perturbation in the oxidative capacity of the troposphere does result in appreciable changes in the lifetimes of the more long-lived trace gas species, as shown by the increase in the tropospheric lifetime of CH_4 by up to $\sim 0.54\,\mathrm{yr}$ (or $\sim 6.1\,\%$), depending on the assumed uptake efficiency.

Comparing the individual heterogeneous loss terms for HO_2 (Table 7) shows that when assuming an equal uptake efficiency for cloud droplets and aerosol as in AER-CLD, the dominant contribution towards the heterogeneous sink term for HO_2 ($\sim 70\,\%$) is due to loss on cloud droplets as a result of the large SAD and the distribution in both hemispheres, with loss on aerosol surfaces contributing $\sim 30\,\%$. Even though the aerosol SAD is much smaller than cloud droplet SAD (see Fig. 2) the contribution to the total HO_2 uptake is still $\sim 30\,\%$, which can be explained as high aerosol loadings appear co-located with high concentrations of HO_2. For AER-S-CLD the HO_2 loss by aerosol uptake increases to $\sim 47\,\%$ of the total uptake, which should be considered as an upper limit of the expected impact. The total uptake on cloud and aerosol is ~ 30–$50\,\%$ of the HO_2 loss related to the O_3 production from NO_x recycling (c.f. AER-CLD

ACPD
14, 8575–8632, 2014

and AER-S-CLD). Furthermore, the magnitude of HO_2 uptake on cloud and aerosol appears largely additive, which indicates that these processes do not compete due to the vertical distribution of the different surface types.

Table 8 presents a zonal breakdown of the O_3 production and loss budget terms for the NH (30–90° N), tropics (30° S–30° N) and SH (30–90° S), which indicates that in absolute terms the impact of HO_2 uptake on aerosol and cloud on the O_3 budget is largest in the tropical region, where HO_2 concentrations are maximal. Nevertheless, the relative decrease of the annual mean chemical O_3 production in the runs with HO_2 uptake remains larger over the extra-tropical SH and NH compared to the tropics. This is because the relative contribution of HO_2 uptake on aerosol and/or cloud, compared to the total HO_2 chemical budget, is smaller in the tropics than in the extra-tropics, and, consequently, the relative decrease of the O_3 production term from NO_x recycling is lower in the tropics (Mao et al., 2013).

The relative decrease in the integrated chemical production and loss terms for tropospheric O_3 in the runs is generally larger for the NH extra-tropics as compared to the SH extra-tropics, related to higher aerosol concentrations. The maximum decrease in O_3 production by up to ~ 10 % is found for run AER-S-CLD over the NH extra-tropics (cf. Fig. 5).

Figure 7 shows the annual average relative differences in the zonal mean values of tropospheric O_3 and CO between the runs AER, AER-CLD and AER-S-CLD with respect to BASE for 2008. While the zonal and annual integrated tropospheric O_3 production and loss terms decrease by similar absolute amounts, locally this is not the case, leading to changes in the spatial distribution of O_3. For example, over the northern mid-latitudes the zonal mean O_3 mixing ratios decrease on average by up to ~ 4 % in run AER-S-CLD, and are approximately localized near the regions which exhibit high NO_x emissions. Also during the NH winter season, with a relatively large abundance of NO, this results in lower net O_3 production, while O_3 effectively increases during the NH summer period by up to ~ 6 % at high northern latitudes. For the SH, O_3 increases for all seasons over the remote regions, e.g., up to ~ 6 % over Antarctica.

ACPD
14, 8575–8632, 2014

In Fig. 8 we evaluate co-located vertical O_3 profiles from BASE and AER-S-CLD against annual composites assembled from ozone sonde profiles for selected WOUDC stations (see Sect 2.3 for further details). To aid clarity we limit the comparisons to BASE and AER-S-CLD only, where the other simulations lie in between these two extremes. This evaluation indicates that the modeled O_3 concentrations over the NH stations Tateno and Hohenpeissenberg decrease by a few percent in the lower troposphere, while the opposite holds for the Antarctic station Neumayer. These changes are representative for the evaluation against all WOUDC stations (see discussion for ARCTAS comparisons, Sect 3.3), and imply a slight improvement compared to the BASE run. The annual mean bias of the four runs in the altitude range of 750–400 hPa for these stations is always below 5 ppb, which holds for the majority of available WOUDC ozone sonde stations (not shown).

3.5 Evaluation of tropospheric CO

The changes in the global HO_x budget result in a decrease in the global oxidative capacity and associated increases in the lifetimes of abundant trace gas species such as CH_4 (Table 6). The corresponding changes in the tropospheric CO budget are presented in Table 9. Comparing values between runs shows that the tropospheric CO lifetime increases from ~ 2 % (AER) to ~ 9 % (AER-S-CLD) due to less chemical loss of CO when there is enhanced heterogeneous scavenging of HO_2. The associated increase in the tropospheric burden is between ~ 2 % (AER) and ~ 7 % (AER-S-CLD). Therefore the effects are not directly linear to the total global SAD. Figure 7 shows that the largest relative increase in the CO burden occurs outside the tropics in the mid-latitudes, in line with the regional changes in the O_3 budget as presented in Table 8. In line with the O_3 analysis, the changes in the CO budget due to uptake on aerosol are of similar order of magnitude as uptake on cloud.

To assess the regional differences introduced in various remote regions we compare the simulations with observations of the GMD monitoring network in Fig. 9. The data are averaged on a monthly basis for days where there are available measurements.

ACPD
14, 8575–8632, 2014

In general, accounting for HO_2 loss improves the bias of C-IFS over the NH, which is consistent with evaluation against ARCTAS data (Sect 3.3). For instance, the annual mean bias at Alert station is reduced from −19 ppb (BASE) to −10 ppb (AER-S-CLD). Nevertheless, even when adopting the high end of possible HO_2 uptake efficiencies as in run AER-S-CLD, a bias with respect to the observations remains at these high northern latitudes.

A mixed picture occurs over the tropics, where C-IFS overestimates mean mixing ratios between June to August at Samoa in BASE. This means that the modest increase in the tropospheric burden further degrades the comparison. For other tropical stations, such as Tenerife and Ascension Island, there is an improvement of the bias for AER-S-CLD. Considering the low regional emissions the overestimation at Samoa is likely caused by an increase in the amount of CO which is transported into the region from biomass burning and/or biogenic sources, combined with an increase in the local lifetime. A similar pattern is seen at Syowa on Antarctica, where the annual mean bias increases from 6 ppb (BASE) to 11 ppb (AER-S-CLD). The increase in CO concentrations over the SH in AER-S-CLD compared with AER-CLD is smaller than over the NH, suggesting that varying uptake efficiencies on different aerosol types could help to explain local biases, although further experimental studies related to this are needed to justify the application of such variations in global CTMs. Nevertheless, there is a general increase in bias over the SH, which constrains a realistic efficiency of HO_2 uptake on clouds and aerosol on a global scale. This is different to a previous global modeling study by Mao et al. (2013), which has predominantly focused on the improvements which occur in the NH, and especially the high northern latitudes, which are additionally sensitive to uncertainties in anthropogenic emission estimates (e.g., Stein et al., 2014).

In order to investigate the impact in the middle troposphere and analyze regional biases we present the global distribution of CO in AER-S-CLD against MOPITT-V6 multispectral TIR/NIR retrievals in Fig. 10, where the details of the measurements are described in Sect. 2.3. This figure illustrates the spatial distribution of CO in C-IFS and

ACPD
14, 8575–8632, 2014

can be used to further examine origins of prevailing CO biases. The NH boreal winter bias observed at the surface (cf. Fig. 8) remains visible in April agreeing with the findings shown for the ARCTAS data (Fig. 5). This bias is highest over the Eastern US, the Eurasian continent and, especially, eastern China. The latter is possibly related to biases in (anthropogenic) emissions (e.g., Miyazaki et al., 2012). Over the tropics, high biases are especially visible over Indonesia (April) and the western part of South America (August). This may be related to uncertainties in the isoprene emissions and chemical degradation, further enhanced with potential biases in the GFAS emissions. The annual and global mean total columns of CO for the other runs are on average lower by up to $\sim 8 \times 10^{16}$ molec cm^{-2} (BASE), i.e., AER-S-CLD features the lowest negative bias over the NH, whereas BASE provides the best correlation at other locations. As the lifetime of CO is ~ 50 days the spatial distribution of the biases is very similar between the runs.

4 Further discussion

The predominant uncertainties associated with are the parameterizations for calculating the distribution and magnitude of cloud and aerosol SAD, and, more importantly, the respective values adopted for describing efficiency of the heterogeneous uptake.

The magnitude of uptake on cloud droplets scales linearly with the available cloud SAD, which in turn depends on cloud properties such as the effective cloud radius ($r_{\mathrm{e,\,cloud}}$). Our parameterization for $r_{\mathrm{e,\,cloud}}$ assumes a linear relationship with respect to the liquid water path (Fouquart et al., 1990), hence taking into account that $r_{\mathrm{e,\,cloud}}$ may exhibit an increase towards the cloud top (Martin et al., 1994). Here we refrain from a systematic evaluation of the cloud SAD due to the difficulty in obtaining accurate global distributions throughout the troposphere. However, the distribution of $r_{\mathrm{e,\,cloud}}$ values seems plausible, being ~ 10 µm over the tropics and the SH storm tracks, decreasing to ~ 6 µm towards the northern latitudes where there are more cloud condensation nuclei available. This appears within the range of SEVIRI observations, such as those

ACPD
14, 8575–8632, 2014

reported in Greuell et al. (2011). Assuming a reasonable cloud representation in the model (Forbes et al., 2011), furthermore initialized by using assimilated meteorology on a daily basis, does place some constraints on the uncertainty in liquid and ice cloud SAD on a global scale.

The uncertainties associated with the aerosol SAD are strongly dependant on the underlying aerosol concentrations and size distributions which are defined in the aerosol scheme. With respect to sea salt aerosol we note that persistent high biases have been reported in an assessment of the MACC reanalysis product (Eskes et al., 2013). This is most clearly observed for sea salt over the SH storm tracks, where an over-estimation of $\sim 100\,\%$ is possible over the SH oceans. If true, this would decrease the impact of aerosol SAD over the SH, thus potentially lowering the positive bias in CO shown in Fig. 8 at Antarctic stations. Nevertheless, the uptake on cloud droplets still remains the dominating term here. For other regions over the globe persistent biases of the MACC reanalysis aerosol distributions exist, including a potential high bias in aerosol SAD over the Arctic when compared to Olson et al. (2012), suggesting that the actual HO_2 uptake on aerosol may be lower than found in our results. Also possible errors in the speciation and vertical distribution of the aerosol loading are not corrected for by the data assimilation system, which could be the cause of the relatively large enhancement of HO_2 uptake on SO_4^{2-}, BC and NO_3^- aerosol over the SH. However, we do have confidence that the MACC reanalysis is able to capture occurrences of high aerosol loadings, as constrained by the MODIS observations of AOD. These strong aerosol signals originate from anthropogenic pollution, desert dust and biomass burning events, and act as the most significant sources of global aerosol SAD. The biases from these sources are generally of the order $\sim$ 10–20 % on an annual and global mean basis, although for individual events biases can be significantly larger. Uncertainties in the parameterization of the effective aerosol particle radius and hygroscopic growth are probably more significant and can add to an additional uncertainty of $\sim 30\,\%$ to the aerosol SAD.

ACPD
14, 8575–8632, 2014

Nevertheless, the largest uncertainty is still related to the assumptions regarding the actual value of $\gamma(HO_2)$ upon any one type of heterogeneous aerosol surface due to the diverse nature associated with the composition of aerosols. Based on observational evidence, values for different aerosol types can range from < 0.01 on ammonium sulphate aerosol at room temperature (Mozurkewich et al., 1987), to 0.4–0.7 on anthropogenic aerosol containing TMI (Taketani et al., 2012; Liang et al., 2013). As of yet it remains unclear to what extent TMI contribute to the total aerosol mass and how they modify the efficiency of HO_2 uptake across the range of pH and chemical composition contained in aerosol particles. The speciation contained in both deliquescent aerosols and dilute solution alters its reactivity towards the reaction efficiency with aquated HO_x radicals, where e.g. iron rarely exists in its fully aquated form in the presence of other solutes with attach themselves as ligands to the TMI (Tilgner et al., 2005).

As pointed out in Mao et al. (2013) and Liang et al. (2013), whether or not the loss at the surface reaction produces additional gas-phase precursors is essential to assess the effect of this heterogeneous reaction, as by assuming H_2O_2 is not formed, the HO_2 uptake is essentially a first-order loss term in the global HO_x budget. However, previous measurements have shown that in more dilute solution reactions in the aqueous phase can act as global sources of H_2O_2 which questions this assumption (Zuo and Hoigne, 1993).

Assuming a global constant value for $\gamma(HO_2)$ of 0.06 for aerosol and liquid cloud, as done in this study, is chosen as a lower limit so as not to exaggerate global effects. Given that the uptake value on cloud droplets is based on few studies, and that any loss on cloud is important at global scale, implies that further laboratory studies should be conducted to see if more modern detection techniques can corroborate this low uptake value. The run with $\gamma(HO_2)$ of 0.7 on a limited set of aerosol types shows the high end of the range of possible uptake efficiencies. However, although this $\gamma(HO_2)$ was selected from the literature based on observational studies (Taketani et al., 2012; Liang et al., 2013), this enhanced uptake value is probably too high to be applied across

ACPD
14, 8575–8632, 2014

specific aerosol types under all chemical regimes (e.g. McNeill et al., 2006), suggesting localized variability in the $\gamma(HO_2)$.

Following the same line of argumentation, the uptake of HO_2 in clouds has been observed by Commane et al. (2010) and is has also been considered in comprehensive aqueous phase chemistry modeling studies (e.g., Williams et al., 2002; Tilgner et al., 2005), although its efficiency on global scale still remains highly uncertain. Having a conservative value for $\gamma(HO_2)$ on liquid clouds also prevents from an over-estimation of the HO_x loss due to subgrid-scale effects in grid cells that are only partly filled with clouds (Jacob, 2000).

5 Conclusions

In this study we quantify the importance of the heterogeneous scavenging of HO_2 on aerosol relative to that on cloud droplet and ice particle surfaces and evaluate the impact on the global oxidative capacity. For this purpose we use C-IFS, where the modified CB05 mechanism has been introduced to model tropospheric chemistry within ECMWF's data assimilation and Integrated Forecast System. While meteorology is constrained by operational analyses, aerosol concentrations are initialized daily from the MACC reanalysis using MODIS observations of AOD, which puts constrains on the total aerosol column, but not its composition.

In this study we assume a conservative, globally constant value $\gamma(HO_2)$ of 0.06 for aerosol and liquid cloud, which can be considered a lower limit. Considering that no consensus has yet reached on observational evidence of HO_2 uptake on different types of aerosol and cloud, there is growing evidence of enhanced uptake on anthropogenic aerosol. Thus we have included a simulation with $\gamma(HO_2)$ of 0.7 on aerosol types associated with anthropogenic sources (SO_4^{2-}, NO_3^-, BC), which is estimated as a reasonable upper limit constrained by observations.

We show that the maximum cloud SAD is typically an order of magnitude larger than that for aerosol SAD, while the spatial distribution is different. Aerosol SAD is largest

ACPD
14, 8575–8632, 2014

near the surface close to its emission sources, which collocates with the regions where most HO_2 is present. Cloud SAD maximizes at ~ 800 hPa over the mid-latitude storm tracks and in tropical convective systems. We quantify the contribution of cloud uptake as much as ~ 53–70 % of the total uptake, depending on the assumptions regarding $\gamma(HO_2)$, due to the ubiquitous presence of cloud droplets. Although the spatial distribution is different, it implies that HO_2 uptake on cloud is complementary to aerosol uptake and may not be neglected in chemistry transport models which otherwise include aerosol uptake.

When adopting this approach our simulations suggest that the zonal mean values for HO_2 are reduced by up to ~ 25 % within the tropics, where in absolute terms most HO_2 uptake takes place, and by up to ~ 40 % in the extra-tropics, where the HO_2 uptake is relatively more important to the HO_x budget. Applying enhanced uptake on anthropogenic aerosol leads to a general reduction of HO_2 which is largest over the extra-tropical Northern Hemisphere by up to 50 % compared to the base run without HO_2 uptake, maximizing over the highly polluted East Asian region.

A comparison against ARCTAS flight data over the Arctic shows that HO_2 mixing ratios are decreased by up to ~ 30 %. This leads to a negative bias during April and June–July 2008, although the simulations remain within the uncertainty range of aircraft observations. The negative bias in HO_2 can, in part, be explained by local biases in modeled H_2O_2 and other HO_2 precursor trace gases. Despite these limitations the evaluation against ARCTAS campaign is valuable as it provides a critical benchmark of the model performance in terms of HO_2 and its precursors.

On average O_3 concentration changes are within a few percent, depending on season and region, with the largest changes over polluted regions (decreases up to 4 %) and high latitudes (increases up to ~ 6 %). The O_3 overall tropospheric production and loss budgets decrease by up to ~ 6 %. The CH_4 lifetime increases by a similar amount towards 9.4 yr. The decrease in oxidative capacity leads to a global increase of CO burden of up to ~ 7 %, where the largest changes are again found outside the tropics. This increase implies an improvement against CO observations over the NH, although

ACPD
14, 8575–8632, 2014

it does not fully resolve the NH wintertime bias. At the same time it increases the high bias over the SH. This constraints the assumptions regarding HO_2 uptake on a global scale. Nevertheless, we show that the use of higher values for $\gamma(HO_2)$ on selective aerosol components prevailing over the NH could contribute to reductions in local biases. Biases in tropospheric O_3 against WOUDC sonde observations are slightly improved and remain generally below 5 ppbv.

Model biases in CH_2O and higher hydrocarbons during April 2008 over the Arctic indicate missing emission sources, which could contribute to the general bias in model CO. Also an evaluation against MOPITT-v6 CO total columns highlight other possible model deficiencies at various regions over the globe, that may contribute to the general biases, e.g. uncertainties in isoprene emissions and chemistry, and uncertainties in anthropogenic emissions over various regions.

Despite the apparent importance of HO_2 heterogeneous chemistry on both clouds and aerosol, large uncertainties remain in many aspects of this modeling approach, including the parameterization of cloud SAD, the actual aerosol composition and its associated SAD, and their respective interactions to trace gases through heterogeneous chemistry. To improve these modeling components, observational evidence is needed regarding the specification of such heterogeneous chemistry on prevailing aerosol and cloud types.

Also an improved description of the modeled aerosol composition can lead to better constraints on the impact of heterogeneous chemistry on tropospheric composition, and hence lead to improvements of the analysis and forecast of atmospheric composition in C-IFS.

Acknowledgements. The MACC-II project has received funding from the European Union's Seventh Framework Programme (FP7) under Grant Agreement no. 283576. We would like to thank the assistance of the many individuals who made the ARCTAS campaign a success, and are grateful to the ARCTAS team who kindly made the observational data available. MOPITT data were obtained from the NASA Langley Research Center Atmospheric Science Data Center. We are grateful to the WOUDC community for making their ozone sonde data available. The NOAA-ESRL GMD is acknowledged for providing CO surface measurement data.

ACPD
14, 8575–8632, 2014

References

Aan de Brugh, J. M. J., Schaap, M., Vignati, E., Dentener, F., Kahnert, M., Sofiev, M., Huijnen, V., and Krol, M. C.: The European aerosol budget in 2006, Atmos. Chem. Phys., 11, 1117–1139, doi:10.5194/acp-11-1117-2011, 2011.

Abbatt, J. P. D., Lee, A. K. Y., and Thornton, J. A.: quantifying trace gas uptake to tropospheric aerosol: recent advances and remaining challenges, Chem. Soc. Rev., 41, 6555–6581, doi:10.1039/c2cs35052a, 2012.

Anastasio, C., Faust, B. C., and Allen, J. M.: Aqueous phase photochemical formation of hydrogen peroxide in authentic cloud waters, J. Geophys. Res., 99, 8231–8248, 1994.

Arakaki, T., Anastasio, C., Shu, P. G., and Faust, B. C.: Aqueous-phase photo production of hydrogen peroxide in authentic cloud waters: wavelength dependence, and the effects of filtration and freeze–thaw cycles, Atmos. Environ., 29, 1697–1703, 1995.

Bellouin, N., Quaas, J., Morcrette, J.-J., and Boucher, O.: Estimates of aerosol radiative forcing from the MACC re-analysis, Atmos. Chem. Phys., 13, 2045–2062, doi:10.5194/acp-13-2045-2013, 2013.

Benedetti, A., Morcrette, J.-J., Boucher, O., Dethof, A., Engelen, R. J., Fisher, M., Flentje, H., Huneeus, N., Jones, L., Kaiser, J. W., Kinne, S., Mangold, A., Razinger, M., Simmons, A. J., and Suttie, M.: Aerosol analysis and forecast in the European Centre for Medium-Range Weather Forecasts Integrated Forecast System: 2. Data assimilation, J. Geophys. Res., 114, D13205, doi:10.1029/2008JD011115, 2009.

Bielski, B. H. J., Cabelli, D. E., Arudi, R. L., and Ross, A. B.: Reactivity of HO_2/O_2-radicals in aqueous solution. J. Phys. Chem. Ref. Data, 14, 1041–1100, 1985.

Chin, M., Ginoux, P., Kinne, S., Torres, O., Holben, B. N., Duncan, B. N., Martin, R. V., Logan, J. A., Higurashi, A., and Nakajima, T.: Tropospheric aerosol optical thickness from the GOCART model and comparisons with satellite and sun photometer measurements, J. Atmos. Sci., 59, 461–483, 2002.

Commane, R., Floquet, C. F. A., Ingham, T., Stone, D., Evans, M. J., and Heard, D. E.: Observations of OH and HO_2 radicals over West Africa, Atmos. Chem. Phys., 10, 8783–8801, doi:10.5194/acp-10-8783-2010, 2010.

Cooper, P. L. and Abbatt, J. P. D.: Heterogeneous interactions of OH and HO_2 radicals with surfaces characteristic of atmospheric particulate matter, J. Phys. Chem., 100, 2249–2254, 1996.

ACPD
14, 8575–8632, 2014

de Reus, M., Fischer, H., Sander, R., Gros, V., Kormann, R., Salisbury, G., Van Dingenen, R., Williams, J., Zöllner, M., and Lelieveld, J.: Observations and model calculations of trace gas scavenging in a dense Saharan dust plume during MINATROC, Atmos. Chem. Phys., 5, 1787–1803, doi:10.5194/acp-5-1787-2005, 2005.

Deeter, M. N.: MOPITT Version 6 Product User's Guide, Technical Report, NCAR, Boulder, USA, 2013.

Deeter, M. N., Worden, H. M., Edwards, D. P., Gille, J. C., and Andrews, A. E.: Evaluation of MOPITT retrievals of lower-tropospheric carbon monoxide over the United States, J. Geophys. Res.-Atmos., 117, D13306, doi:10.1029/2012JD017553, 2012.

Dubovik, O., Holben, B., Eck, T. F., Smirnov, A., Kaufman, Y., King, M. D., Tanré, D., and Slutsker, I.: variability of absorption and optical properties of key aerosol types observed in worldwide locations, J. Atmos. Sci., 59, 590–608, 2002.

Emmons, L. K., Walters, S., Hess, P. G., Lamarque, J.-F., Pfister, G. G., Fillmore, D., Granier, C., Guenther, A., Kinnison, D., Laepple, T., Orlando, J., Tie, X., Tyndall, G., Wiedinmyer, C., Baughcum, S. L., and Kloster, S.: Description and evaluation of the Model for Ozone and Related chemical Tracers, version 4 (MOZART-4), Geosci. Model Dev., 3, 43–67, doi:10.5194/gmd-3-43-2010, 2010.

Ervens, B., Geroge, C., Williams, J. E., Buxton, G. V., Salmon, G. A., Bydder, M., Wilkinson, F., Dentener, F., Mirabel, P., Wolke, R., and Herrmann, H.: CAPRAM 2.4 (MODAC mechanism): an extended and condensed tropospheric aqueous phase mechanism and its application, J. Geophys. Res., 108, 4426, doi:10.1029/2002JD002202, 2003.

Eskes, H., Huijnen, V., Melas, D., Katragkou, E., Schulz, M., and Lefever, K.: Validation report of the MACC reanalysis of global atmospheric composition: Period 2003–2012, MACC Technical report D_83.5, available at: http://www.gmes-atmosphere.eu/services/gac/global_verification/validation_reports/ (last access: 15 January 2014), 2013.

Flemming, J., Huijnen, V., Stein, O., Arteta, J., and Schultz, M. G.: Atmospheric chemistry in the Integrated Forecast System of ECMWF, in preparation, 2014.

Forbes, R., Tompkins, A. M., and Untch, A.: A new prognostic bulk microphysics scheme for the IFS, Tech. Memo. 649, http://www.ecmwf.int/publications/library/do/references/list/14 (last access: 15 January 2014), ECMWF, 2011.

Fouquart, Y., Buriez, J. C., Herman, M., and Kandel, R. S.: The influence of clouds on radiation: a climate-modelling perspective, Rev. Geophys., 28, 145–166, 1990.

ACPD
14, 8575–8632, 2014

Fu, Q.: An accurate parameterization of the solar radiative properties of cirrus clouds for climate models, J. Climate, 9, 2058–2082, 1996.

George, I. J., Matthews, P. S. J., Whalley, L. K., Brooks, B., Goddard, A., Baeza-Romero, M. T., and Heard, D. E.: Measurements of uptake coefficients for heterogeneous loss of HO_2 onto submicron inorganic salt aerosols, Phys. Chem. Chem. Phys., 15, 12829–12845, doi:10.1039/C3CP51831K, 2013.

Granier, C., Guenther, A., Lamarque, J., Mieville, A., Muller, J., Olivier, J., Orlando, J., Peters, J., Petron, G., Tyndall, G., and Wallens, S.: POET, a database of surface emissions of ozone precursors, available at: http://eccad.sedoo.fr (last access: 15 January 2014), 2005.

Granier, C., Bessagnet, B., Bond, T., D'Angiola, A., Denier van der Gon, H., Frost, G. J., Heil, A., Kaiser, J. W., Kinne, S., Klimont, Z., Kloster, S.-F., Lamarque, J., Liousse, C., Masui, T., Meleux, F., Mieville, A., Ohara, T., Raut, J.-C., Riahi, K., Schultz, M. G., Smith, S. J., Thompson, A., van Aardenne, J., van der Werf, G. R., and van Vuuren, D. P.: Evolution of anthropogenic and biomass burning emissions of air pollutants at global and regional scales during the 1980–2010 period, Climate Change, 109, 163–190, doi:10.1007/s10584-011-0154-1, 2011.

Greuell, W., van Meijgaard, E., Clerbaux, N., and Meirink, J.-F.: Evaluation of model-predicted top-of-atmosphere radiation and cloud parameters over Africa with observations from GERB and SEVIRI, J. Climate, 24, 4015–4036, 2011.

Guenther, A., Karl, T., Harley, P., Wiedinmyer, C., Palmer, P. I., and Geron, C.: Estimates of global terrestrial isoprene emissions using MEGAN (Model of Emissions of Gases and Aerosols from Nature), Atmos. Chem. Phys., 6, 3181–3210, doi:10.5194/acp-6-3181-2006, 2006.

Hanson, D. R. and Ravishankara, A. R.: The reaction probabilities of $ClONO_2$ and N_2O_5 on polar stratospheric cloud materials, J. Geophys. Res., 96, 5081–5090, 1991.

Heymsfield, A. J. and McFarquhar, G. M.: High Albedos of cirrus in the tropical pacific warm pool: microphysical interpretations from CEPEX and from Kwajalein, Marshall Islands, J. Atmos. Sci., 53, 2424–2451, doi:10.1175/1520-0469(1996)053<2424:HAOCIT>2.0.CO;2, 1996.

Hornbrook, R. S., Blake, D. R., Diskin, G. S., Fried, A., Fuelberg, H. E., Meinardi, S., Mikoviny, T., Richter, D., Sachse, G. W., Vay, S. A., Walega, J., Weibring, P., Weinheimer, A. J., Wiedinmyer, C., Wisthaler, A., Hills, A., Riemer, D. D., and Apel, E. C.: Observations of nonmethane organic compounds during ARCTAS – Part 1: Biomass burning emis-

ACPD
14, 8575–8632, 2014

sions and plume enhancements, Atmos. Chem. Phys., 11, 11103–11130, doi:10.5194/acp-11-11103-2011, 2011.

Huijnen, V., Williams, J., van Weele, M., van Noije, T., Krol, M., Dentener, F., Segers, A., Houweling, S., Peters, W., de Laat, J., Boersma, F., Bergamaschi, P., van Velthoven, P., Le Sager, P., Eskes, H., Alkemade, F., Scheele, R., Nédélec, P., and Pätz, H.-W.: The global chemistry transport model TM5: description and evaluation of the tropospheric chemistry version 3.0, Geosci. Model Dev., 3, 445–473, doi:10.5194/gmd-3-445-2010, 2010.

Huijnen, V., Flemming, J., Kaiser, J. W., Inness, A., Leitão, J., Heil, A., Eskes, H. J., Schultz, M. G., Benedetti, A., Hadji-Lazaro, J., Dufour, G., and Eremenko, M.: Hindcast experiments of tropospheric composition during the summer 2010 fires over western Russia, Atmos. Chem. Phys., 12, 4341–4364, doi:10.5194/acp-12-4341-2012, 2012.

Jacob, D. J., Crawford, J. H., Maring, H., Clarke, A. D., Dibb, J. E., Emmons, L. K., Ferrare, R. A., Hostetler, C. A., Russell, P. B., Singh, H. B., Thompson, A. M., Shaw, G. E., McCauley, E., Pederson, J. R., and Fisher, J. A.: The Arctic Research of the Composition of the Troposphere from Aircraft and Satellites (ARCTAS) mission: design, execution, and first results, Atmos. Chem. Phys., 10, 5191–5212, doi:10.5194/acp-10-5191-2010, 2010.

Jacob, J. D.: Heterogeneous chemistry and tropospheric ozone, Atmos. Environ., 34, 2131–2159, 2000.

Kaiser, J. W., Heil, A., Andreae, M. O., Benedetti, A., Chubarova, N., Jones, L., Morcrette, J.-J., Razinger, M., Schultz, M. G., Suttie, M., and van der Werf, G. R.: Biomass burning emissions estimated with a global fire assimilation system based on observed fire radiative power, Biogeosciences, 9, 527–554, doi:10.5194/bg-9-527-2012, 2012.

Kolb, C. E., Cox, R. A., Abbatt, J. P. D., Ammann, M., Davis, E. J., Donaldson, D. J., Garrett, B. C., George, C., Griffiths, P. T., Hanson, D. R., Kulmala, M., McFiggans, G., Pöschl, U., Riipinen, I., Rossi, M. J., Rudich, Y., Wagner, P. E., Winkler, P. M., Worsnop, D. R., and O' Dowd, C. D.: An overview of current issues in the uptake of atmospheric trace gases by aerosols and clouds, Atmos. Chem. Phys., 10, 10561–10605, doi:10.5194/acp-10-10561-2010, 2010.

Lamarque, J.-F., Bond, T. C., Eyring, V., Granier, C., Heil, A., Klimont, Z., Lee, D., Liousse, C., Mieville, A., Owen, B., Schultz, M. G., Shindell, D., Smith, S. J., Stehfest, E., Van Aardenne, J., Cooper, O. R., Kainuma, M., Mahowald, N., McConnell, J. R., Naik, V., Riahi, K., and van Vuuren, D. P.: Historical (1850–2000) gridded anthropogenic and biomass burn-

ACPD
14, 8575–8632, 2014

ing emissions of reactive gases and aerosols: methodology and application, Atmos. Chem. Phys., 10, 7017–7039, doi:10.5194/acp-10-7017-2010, 2010.
Lelieveld, J. and Crutzen, P.: The role of clouds in tropospheric photochemistry, J. Atmos. Chem., 12, 229–267, 1991.
Liang, H., Chen, Z. M., Huang, D., Zhao, Y., and Li, Z. Y.: Impacts of aerosols on the chemistry of atmospheric trace gases: a case study of peroxides and HO_2 radicals, Atmos. Chem. Phys., 13, 11259–11276, doi:10.5194/acp-13-11259-2013, 2013.
Liang, J. and Jacob, D. J.: Effect of aqueous phase cloud chemistry on tropospheric ozone, J. Geophys. Res., 102, 5993–6001, doi:10.1029/96JD02957, 1997.
Liao, H. and Seinfeld, J. H.: Global impacts of gas-phase chemistry-aerosol interactions on direct radiative forcing by anthropogenic aerosols and ozone, J. Geophys. Res., 110, D18208, doi:10.1029/2005JD005907, 2005.
Lin, J.-T., Liu, Z., Zhang, Q., Liu, H., Mao, J., and Zhuang, G.: Modeling uncertainties for tropospheric nitrogen dioxide columns affecting satellite-based inverse modeling of nitrogen oxides emissions, Atmos. Chem. Phys., 12, 12255–12275, doi:10.5194/acp-12-12255-2012, 2012.
Logan, J. A., Prather, M. J., Wofsy, S. C., and McElroy, M. B.: Tropospheric chemistry: a global perspective, J. Geophys. Res., 86, 7210–7254, doi:10.1029/JC086iC08p07210, 1981.
Loukhovitskaya, E., Bedjanian, Y., Morozov, I., and Le Bras, G.: Laboratory study of the interaction of HO_2 radicals with the NaCl, NaBr, $MgCl_2 \cdot 6H_2O$ and sea salt surfaces, Phys. Chem. Chem. Phys., 11, 7896–7905, doi:10.1039/B906300E, 2009.
Macintyre, H. L., and Evans, M. J.: Parameterisation and impact of aerosol uptake of HO_2 on a global tropospheric model, Atmos. Chem. Phys., 11, 10965–10974, doi:10.5194/acp-11-10965-2011, 2011.
Mao, J., Jacob, D. J., Evans, M. J., Olson, J. R., Ren, X., Brune, W. H., Clair, J. M. St., Crounse, J. D., Spencer, K. M., Beaver, M. R., Wennberg, P. O., Cubison, M. J., Jimenez, J. L., Fried, A., Weibring, P., Walega, J. G., Hall, S. R., Weinheimer, A. J., Cohen, R. C., Chen, G., Crawford, J. H., McNaughton, C., Clarke, A. D., Jaeglé, L., Fisher, J. A., Yantosca, R. M., Le Sager, P., and Carouge, C.: Chemistry of hydrogen oxide radicals (HO_x) in the Arctic troposphere in spring, Atmos. Chem. Phys., 10, 5823–5838, doi:10.5194/acp-10-5823-2010, 2010.

ACPD
14, 8575–8632, 2014

Mao, J., Fan, S., Jacob, D. J., and Travis, K. R.: Radical loss in the atmosphere from Cu-Fe redox coupling in aerosols, Atmos. Chem. Phys., 13, 509–519, doi:10.5194/acp-13-509-2013, 2013.

Marinoni, A., Parazols, M., Brigante, M., Deguillaume, L., Amato, P., Delort, A.-M., Laj, P., and Mailhot, G.: Hydrogen peroxide in natural cloud water: sources and photoreactivity, Atmos. Res., 101, 256–263, doi:10.1016/j.atmosres.2011.02.013, 2011.

Martin, G. M., Johnson, D. W., and Spice, A.: The measurement and parameterization of effective radius of droplets in warm stratocumulus clouds, J. Atmos. Sci., 51, 1823–1842, 1994.

Martin, R. V., Jacob, D. J., Yantosca, R. M., Chin, M., and Ginoux, P.: Global and regional decreases in tropospheric oxidants from photochemical effects of aerosols, J. Geophys. Res., 108, 4097, doi:10.1029/2002JD002622, 2003.

McNeill, V. F., Patterson, J., Wolfe, G. M., and Thornton, J. A.: The effect of varying levels of surfactant on the reactive uptake of N_2O_5 to aqueous aerosol, Atmos. Chem. Phys., 6, 1635–1644, doi:10.5194/acp-6-1635-2006, 2006.

Metzger, S., Dentener, F., Pandis, S., and Lelieveld, J.: Gas/aerosol partitioning, 1, A computationally efficient model, J. Geophys. Res., 107, ACH 16-1–ACH 16-24, doi:10.1029/2001JD001102, 2002.

Michou, M., Laville, P., Serça, D., Fotiadi, A., Bouchou, P., and Peuch, V.-H.: Measured and modeled dry deposition velocities over the ESCOMPTE area, Atmos. Res., 74, 89–116, doi:10.1016/j.atmosres.2004.04.011, .

Miyazaki, K., Eskes, H. J., Sudo, K., Takigawa, M., van Weele, M., and Boersma, K. F.: Simultaneous assimilation of satellite NO_2, O_3, CO, and HNO_3 data for the analysis of tropospheric chemical composition and emissions, Atmos. Chem. Phys., 12, 9545–9579, doi:10.5194/acp-12-9545-2012, 2012.

Morcrette, J.-J., Boucher, O., Jones, L., Salmond, D., Bechtold, P., Beljaars, A., Benedetti, A., Bonet, A., Kaiser, J. W., Razinger, M., Schulz, M., Serrar, S., Simmons, A. J., Sofiev, M., Suttie, M., Tompkins, A. M., and Untch, A.: Aerosol analysis and forecast in the European Centre for Medium-Range Weather Forecasts Integrated Forecast System: forward modeling, J. Geophys. Res., 114, D06206, doi:10.1029/2008JD011235, 2009.

Morcrette, J.-J., Benedetti, A., Jones, L., Kaiser, J. W., Razinger, M., and Suttie, M.: Prognostic aerosols in the ECMWF IFS: MACC vs. GEMS aerosols, TechMemo 659, http://www.ecmwf.int/publications/library/do/references/list/14 (last access: 15 January 2014), ECMWF, 2011.

ACPD
14, 8575–8632, 2014

Morita, A., Kanaya, Y., and Francisco, J. S.: Uptake of the HO_2 radical by water: molecular dynamics calculations and their implications for atmospheric modeling, J. Geophys. Res., 109, D09201, doi:10.1029/2003JD004240, 2004.
Mozurkewich, M., McMurray, P. H., Guppta, A., and Calvert, J. G.: Mass accommodation coefficient for HO_2 radicals on aqueous particles, J. Geophys. Res., 92, 4163–4170, 1987
Myhre, G., Samset, B. H., Schulz, M., Balkanski, Y., Bauer, S., Berntsen, T. K., Bian, H., Bellouin, N., Chin, M., Diehl, T., Easter, R. C., Feichter, J., Ghan, S. J., Hauglustaine, D., Iversen, T., Kinne, S., Kirkevåg, A., Lamarque, J.-F., Lin, G., Liu, X., Lund, M. T., Luo, G., Ma, X., van Noije, T., Penner, J. E., Rasch, P. J., Ruiz, A., Seland, Ø., Skeie, R. B., Stier, P., Takemura, T., Tsigaridis, K., Wang, P., Wang, Z., Xu, L., Yu, H., Yu, F., Yoon, J.-H., Zhang, K., Zhang, H., and Zhou, C.: Radiative forcing of the direct aerosol effect from AeroCom Phase II simulations, Atmos. Chem. Phys., 13, 1853–1877, doi:10.5194/acp-13-1853-2013, 2013.
Olivier, J., Peters, J., Granier, C., Petron, G., Müller, J., and Wallens, S.: Present and future surface emissions of atmospheric compounds, POET report #2, EU project EVK2-1999-00011, available at: http://eccad.sedoo.fr (last access: 15 January 2014), 2003.
Olson, J. R., Crawford, J. H., Brune, W., Mao, J., Ren, X., Fried, A., Anderson, B., Apel, E., Beaver, M., Blake, D., Chen, G., Crounse, J., Dibb, J., Diskin, G., Hall, S. R., Huey, L. G., Knapp, D., Richter, D., Riemer, D., Clair, J. St., Ullmann, K., Walega, J., Weibring, P., Weinheimer, A., Wennberg, P., and Wisthaler, A.: An analysis of fast photochemistry over high northern latitudes during spring and summer using in-situ observations from ARCTAS and TOPSE, Atmos. Chem. Phys., 12, 6799–6825, doi:10.5194/acp-12-6799-2012, 2012.
Parazois, M., Marinoni, A., Amato, P., Abida, O., Laj, P., and Mailhot, G.: Speciation and role of iron in cloud droplets at the puy de Dome station, J. Atmos. Chem., 54, 267–281, 2006.
Popp, P. J., Gao, R. S., Marcy, T. P., Fahey, D. W., Hudson, P. K., Thompson, T. L., Kärcher, B., Ridley, B. A., Weinheimer, A. J., Knapp, D. J., Montzka, D. D., Baumgardner, D., Garrett, T. J., Weinstock, E. M., Smith, J. B., Sayres, D. S., Pittman, J. V. Dhaniyala, S., Bui T. P., and Mahoney, M. J.: Nitric acid uptake on subtropical cirrus cloud particles, J. Geophys. Res., 109, D06302, doi:10.1029/2003JD004255, 2004.
Pozzoli, L., Bey, I., Rast, S., Schultz, M. G., Stier, P., and Feichter, J.: Trace gas and aerosol interactions in the fully coupled model of aerosol-chemistry-climate ECHAM5-HAMMOZ: 1. Model description and insights from the spring 2001 TRACE-P experiment, J. Geophys. Res., 113, D07308, doi:10.1029/2007JD009007, 2008.

ACPD
14, 8575–8632, 2014

Prather, M. J., Holmes, C. D., and Hsu, J.: Reactive greenhouse gas scenarios: systematic exploration of uncertainties and the role of atmospheric chemistry, Geophys. Res. Lett., 39, L09803, doi:10.1029/2012GL051440, 2012.

Remer, L. A., Kaufman, Y. J., Tanré, D., Mattoo, S., Chu, D. A., Martins, J. V., Li, R.-R., Ichoku, C., Levy, R. C., Kleidman, R. G., Eck, F., Vermote, E., and Holben, B. N.: The MODIS aerosol algorithm, products, and validation, J. Atmos. Sci., 62, 947–973, doi:10.1175/JAS3385.1, 2005.

Sanderson, M. G., Collins, W. J., Derwent, R. G., and Johnson, C. E.: Simulation of global hydrogen levels using a Lagrangian Three-Dimensional Model, J. Atmos. Chem., 46, 15–28, doi:10.1023/A:1024824223232, 2003.

Schmitt, C. G. and Heymsfield, A. J.: Total surface area estimates for individual ice particles and particle populations, J. Appl. Meteorol., 44, 467–474, 2005.

Schwartz, S. E.: Mass-transport considerations pertinent to aqueous-phase reactions of gases in liquid-water clouds, in: Chemistry of Multiphase Atmospheric Systems, edited by: Jaechske, W., Springer, Heidelberg, 415–471, 1986.

Stein, O., Schultz, M. G., Bouarar, I., Clark, H., Huijnen, V., Gaudel, A., George, M., and Clerbaux, C.: On the wintertime low bias of Northern Hemisphere carbon monoxide in global model studies, Atmos. Chem. Phys. Discuss., 14, 245–301, doi:10.5194/acpd-14-245-2014, 2014.

Stevenson, D. S., Dentener, F. J., Schultz, M. G., Ellingsen, K., van Noije, T. P. C., Wild, O., Zeng, G., Amann, M., Atherton, C. S., Bell, N., Bergmann, D. J., Bey, I., Butler, T., Cofala, J., Collins, W. J., Derwent, R. G., Doherty, R. M., Drevet,J., Eskes, H. J., Fiore, A. M., Gauss,M., Hauglustaine,D. A., Horowitz, L. W., Isaksen, I. S. A., Krol,M. C., Lamarque, J.-F., Lawrence, M. G., Montanaro, V., Müller, J.-F., Pitari, G., Prather, M. J., Pyle, J. A., Rast, S., Rodriguez, J. M., Sanderson, M. G., Savage, N. H., Shindell, D. T., Strahan, S. E., Sudo K., and Szopa, S.: Multimodel ensemble simulations of present-day and near-future tropospheric ozone, J. Geophys. Res., 111, D08301, doi:10.1029/2005JD006338, 2006.

Taketani, F., Kanaya, Y., and Akimoto, H.: Kinetics of heterogeneous reactions of HO_2 radical at ambient concentration levels with $(NH_4)_2SO_4$ and NaCl aerosol particles, J. Phys. Chem. A, 112, 2370–2377, 2008.

Taketani, F., Kanaya, Y., and Akimoto, H.: Heterogeneous loss of HO_2 by KCl, synthetic sea salt, and natural seawater aerosol particles, Atmos. Environ., 43, 1660–1665, 2009.

ACPD
14, 8575–8632, 2014

Taketani, F., Kanaya, Y., Pochanart, P., Liu, Y., Li, J., Okuzawa, K., Kawamura, K., Wang, Z., and Akimoto, H.: Measurement of overall uptake coefficients for HO_2 radicals by aerosol particles sampled from ambient air at Mts. Tai and Mang (China), Atmos. Chem. Phys., 12, 11907–11916, doi:10.5194/acp-12-11907-2012, 2012.

Tang, M. J., Thieser, J., Schuster, G., and Crowley, J. N.: Uptake of NO_3 and N_2O_5 to Saharan dust, ambient urban aerosol and soot: a relative rate study, Atmos. Chem. Phys., 10, 2965–2974, doi:10.5194/acp-10-2965-2010, 2010.

Tie, X., Brasseur, G., Emmons, L., Horowitz, L., and Kinnison, D.: Effects of aerosols on tropospheric oxidants: a global model study, J. Geophys. Res., 106, 22931–22964, doi:10.1029/2001JD900206, 2001.

Tie, X., Madronich, S., Walters, S., Edwards, D. P., Ginoux, P., Mahowald, N., Zhang, R., Lou, C., and Brasseur, G., Assessment of the global impact of aerosols on tropospheric oxidants, J. Geophys. Res., 110, D03204, doi:10.1029/2004JD005359, 2005.

Thomas, J. L., Raut, J.-C., Law, K. S., Marelle, L., Ancellet, G., Ravetta, F., Fast, J. D., Pfister, G., Emmons, L. K., Diskin, G. S., Weinheimer, A., Roiger, A., and Schlager, H.: Pollution transport from North America to Greenland during summer 2008, Atmos. Chem. Phys., 13, 3825–3848, doi:10.5194/acp-13-3825-2013, 2013.

Thornton, J., A. and Abbatt, J. P. D.: Measurements of HO_2 uptake to aqueous aerosol: mass accommodation coefficients and net reactive loss, J. Geophys. Res., 110, D08309, doi:10.1029/2004JD005402, 2005.

Thornton, J. A., Jaeglé, L., and McNeill, V. F.: Assessing known pathways for HO_2 loss in aqueous atmospheric aerosols: regional and global impacts on tropospheric oxidants. J. Geophys. Res, 113, D05303, doi:10.1029/2007JD009236, 2008.

Tilgner, A., Majdik, Z., Sehili, A. M., Simmel, M., Wolke, R., and Herrmann, H.: SPACCIM: simulations of the multiphase chemistry occurring in the FEBUKO hill cap cloud experiments, Atmos. Environ., 39, 23–24, 4389–4401, doi:10.1016/j.atmosenv.2005.02.028, 2005.

Vignati, E., Wilson, J., and Stier, P.: M7: an efficient size-resolved aerosol microphysics module for large-scale aerosol transport models, J. Geophys. Res., 109, D22202, doi:10.1029/2003JD004485, 2004.

Wang, Y., Arellanes, C., Curtis, D. B., and Paulson, S. E.: Probing the source of hydrogen peroxide associated with coarse mode aerosol particles in southern California, Environ. Sci. Technol., 44, 4070–4075, 2010.

ACPD
14, 8575–8632, 2014

Whalley, L. K., Furneaux, K. L., Goddard, A., Lee, J. D., Mahajan, A., Oetjen, H., Read, K. A., Kaaden, N., Carpenter, L. J., Lewis, A. C., Plane, J. M. C., Saltzman, E. S., Wiedensohler, A., and Heard, D. E.: The chemistry of OH and HO_2 radicals in the boundary layer over the tropical Atlantic Ocean, Atmos. Chem. Phys., 10, 1555–1576, doi:10.5194/acp-10-1555-2010, 2010.

Williams, J. E., Dentener, F. J., and van den Berg, A. R.: The influence of cloud chemistry on HO_x and NO_x in the moderately polluted marine boundary layer: a 1-D modelling study, Atmos. Chem. Phys., 2, 39–54, doi:10.5194/acp-2-39-2002, 2002.

Williams, J. E., Landgraf, J., Bregman, A., and Walter, H. H.: A modified band approach for the accurate calculation of online photolysis rates in stratospheric-tropospheric Chemical Transport Models, Atmos. Chem. Phys., 6, 4137–4161, doi:10.5194/acp-6-4137-2006, 2006.

Williams, J. E., Strunk, A., Huijnen, V., and van Weele, M.: The application of the Modified Band Approach for the calculation of on-line photodissociation rate constants in TM5: implications for oxidative capacity, Geosci. Model Dev., 5, 15–35, doi:10.5194/gmd-5-15-2012, 2012.

Williams, J. E., van Velthoven, P. F. J., and Brenninkmeijer, C. A. M.: Quantifying the uncertainty in simulating global tropospheric composition due to the variability in global emission estimates of Biogenic Volatile Organic Compounds, Atmos. Chem. Phys., 13, 2857–2891, doi:10.5194/acp-13-2857-2013, 2013.

Yarwood, G., Rao, S., Yocke, M., and Whitten, G.: Updates to the carbon bond chemical mechanism: CB05, Final report to the US EPA, EPA Report Number: RT-0400675, available at: www.camx.com (last access: 15 January 2014), 2005.

Zaveri, R. A. and Peters, L. K.: A new lumped structure photochemical mechanism for large-scale applications, J. Geophys. Res., 104, 30387–30415, doi:10.1029/1999JD900876, 1999.

Zuo, Y. and Hoigne, J.: Formation of hydrogen-peroxide and depletion of oxalic-acid in atmospheric water by photolysis of iron (III) oxalato complexes, Environ. Sci. Technol., 26, 1014–1022, 1992.

ACPD
14, 8575–8632, 2014

Table 1. The dry density and the effective radii of aerosol particles at 0 and 70 % RH for the various aerosol particles included in the C-IFS.

Aerosol type	ρ [g cm^{-3}] RH = 0 %	r_e [µm] RH = 0 %	r_e [µm] RH = 70 %
Sulfate	1.7	0.18	0.25
Nitrate, Ammonium[a]	1.7	0.2	0.27
Black carbon, (hydrophilic)[b]	1.0	0.04	0.04
Organic matter, (hydrophilic)[b]	1.8	0.13	0.18
Sea salt			
0.03–0.5 µm	2.2	0.1	0.18
0.5–5.0 µm	2.2	0.7	1.26
5.0–20 µm	2.2	8	14.4
Desert dust			
0.03–0.55 µm	2.5	0.051	0.051
0.55–0.9 µm	2.5	0.81	0.81
0.9–20 µm	2.5	18	18

[a] $NO3^-$ and NH_4^+ are included for the computation of heterogeneous reactions, but not for AOD.
[b] For hydrophobic black carbon and organic matter the same aerosol properties are assumed as for the hydrophilic types, except that they don't take up water.

ACPD
14, 8575–8632, 2014

Table 2. Extension of the reaction pathways for C_3H_6 and C_3H_8 oxidation, and modification of the isoprene oxidation reaction as adopted in this study, compared to that described in Williams et al. (2013).

$CH_3O_2 + CH_3O_2$	$1.37 \times HCHO + 0.74 \times HO_2 + 0.63 \times CH_3OH$	$9.5 \times 10^{-14} \times \exp(390/T)$
$C_3H_8 + OH$	$IC_3H_7O_2$	$7.6 \times 10^{-12} \times \exp(-585/T)$
$IC_3H_7O_2 + NO$	$0.82CH_3COCH_3 + HO_2 + 0.27ALD2 + NO_2$	$4.2 \times 10^{12} \times \exp(180/T)$
$IC_3H_7O_2 + HO_2$	ROOH	$7.5 \times 10^{13} \times \exp(700/T)$
$C_3H_6 + OH$	HYPROPO2	$k_0 = 8.0 \times 10^{-27} \times (-300/T)^{3.5}$ $k_\infty = 3.0 \times 10^{-11}$
HYPROPO2 + NO	$ALD2 + HCHO + HO_2 + NO_2$	$4.2 \times 10^{12} \times \exp(180/T)$
$HYPROPO2 + HO_2$	ROOH	$7.5 \times 10^{13} \times \exp(700/T)$
$C_5H_8 + OH$	$0.7XO_2 + 0.088XO_2N + 0.629CH_2O + 0.5HO_2 + 0.4ISPD$	$2.7 \times 10^{11} \times \exp(390/T)$

ACPD
14, 8575–8632, 2014

Table 3. Gas-phase emission totals for the year 2008 as applied in the C-IFS. Units are in Tg species yr^{-1} unless otherwise indicated.

Species	Anthro	Bio	BMB
CO	612	96	325
NO_x (Tg N)	32.8	5.0	4.3
CH_2O	3.4	4.0	4.9
CH_3OH	2.2	159	8.5
C_2H_6	3.4	1.1	2.3
C_2H_5OH	3.1	0	0
C_2H_4	7.7	18.0	4.3
C_3H_8	4.0	1.3	1.2
C_3H_6	3.5	7.6	2.5
PAR (Tg C)	30.9	18.1	1.7
OLE (Tg C)	2.4	0.0	0.7
ALD2 (Tg C)	1.1	6.1	2.17
CH_3COCH_3	1.3	28.5	2.4
Isoprene	0	523	0
Terpenes	0	97	0

ACPD
14, 8575–8632, 2014

Table 4. The uptake coefficients applied for N_2O_5 on the various heterogeneous surfaces.

Surface type	γ	Reference
SS, OM, SO_4^{2-}, NO_3^-, NH_4	0.02	Macintyre and Evans (2010)
DD, BC	0.01	Tang et al. (2010)
Liquid cloud	$2.7 \times 10^{-5} \exp(1800/T)$	IUPAC
Ice cloud	0.02	Hanson and Ravishankara (1991)

ACPD
14, 8575–8632, 2014

Table 5. The uptake coefficients used for the heterogeneous scavenging of HO_2 onto various types of particle surface.

Surface type	γ	Reference
SS, DD, OM*	0.06	Abbatt et al. (2012)
SO_4^{2-}, NO_3^-, BC*	0.7	Taketani et al. (2012); Liang et al. (2013)
Liquid cloud	0.06	Kolb et al. (2010)
Ice cloud	0.025	Cooper and Abbatt (1996)

*Note that for sensitivity run "AER" all aerosol, including SO_4^{2-}, NO_3^- and BC, apply a $\gamma(HO_2) = 0.06$.

ACPD
14, 8575–8632, 2014

Table 6. The tropospheric O_3 budget for 2008 (production, loss, deposition, stratospheric inflow), tropospheric burden, lifetime (τ_{O_3}) and associated methane lifetime (τ_{CH_4}) for the four runs. Units are given in $Tg\,O_3\,yr^{-1}$ and $Tg\,O_3$, respectively, where τ_{O_3} is in days and τ_{CH_4} given in years.

	P	L	D	S^*_{infl}	B_{O_3}	τ_{O_3}	τ_{CH_4}
BASE	4494	4227	812	546	367	26.6	8.89
AER	4422	4154	813	546	368	27.1	9.04
AER-CLD	4321	4048	813	540	369	27.8	9.24
AER-S-CLD	4239	3966	810	538	369	28.3	9.43

*The stratospheric inflow is inferred from the residual of the other terms following the approach outlined in Stevenson et al. (2006).

ACPD
14, 8575–8632, 2014

Table 7. The dominant annual global budget terms for HO_2 loss in Tg HO_2 yr^{-1}.

	HO_2 + Aer	HO_2 + CLD	NO + HO_2	O_3 + HO_2	OH + HO_2
BASE	N/A	N/A	2112	890	491
AER	262	N/A	2059	840	474
AER-CLD	240	539	1975	765	438
AER-S-CLD	463	528	1919	714	422

ACPD
14, 8575–8632, 2014

Table 8. Selected annual zonal mean O_3 chemical production and loss budget for the SH (90–30° S), tropics (30° S–30° N) and NH (30–90° N) in $Tg\,O_3\,yr^{-1}$ for run BASE, and percentual changes for the three sensitivity runs with respect to BASE.

	O_3-P SH/Tr/NH	O_3-L SH/Tr/NH
BASE (Tg yr^{-1})	287/3152/1054	283/3113/1025
AER (%)	−1.4/−1.2/−2.8	−1.6/−1.3/−3.5
AER-CLD (%)	−4.2/−2.8/−6.8	−5.2/−3.2/−8.3
AER-S-CLD (%)	−7.4/−4.0/−10.2	−8.7/−4.4/−12.4

ACPD
14, 8575–8632, 2014

Table 9. The tropospheric CO budget (emission, chemical production and loss, dry deposition), burden and lifetime. Units are in Tg CO yr^{-1} and Tg CO, respectively. CO lifetime in days.

	Emis	P	L	D	B_{CO}	τ_{co}
BASE	1036	1503	2395	123	355	51.7
AER	1036	1490	2381	124	362	52.8
CLD-AER	1036	1473	2361	126	370	54.5
CLD-S-AER	1036	1457	2344	128	379	56.1

ACPD
14, 8575–8632, 2014

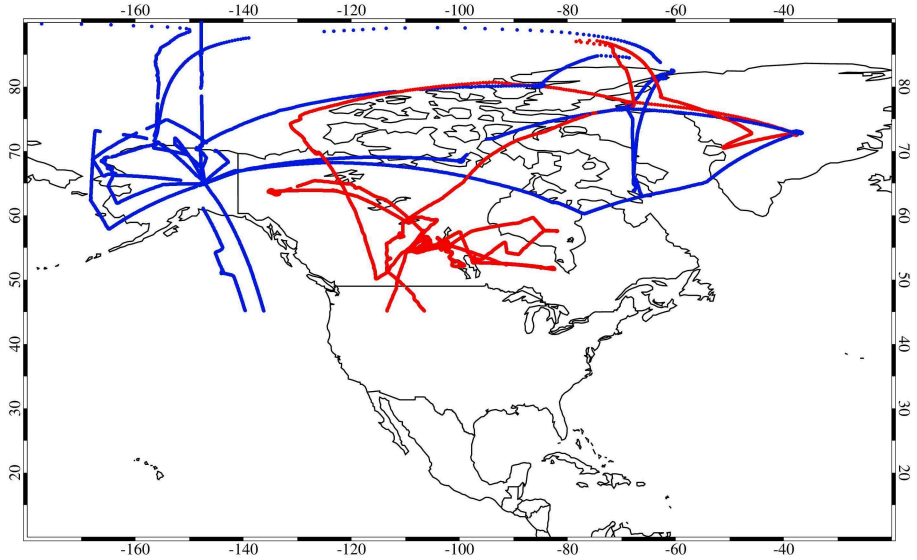

Fig. 1. The geo-location of the ARCTAS flights selected for April (blue) and for June–July (red) used for comparisons with C-IFS trace gas distribution. Only flights North of 45° N are used for the validation of the C-IFS.

ACPD
14, 8575–8632, 2014

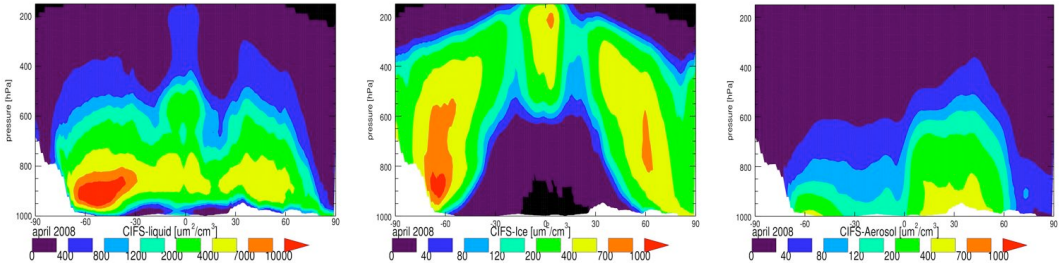

Fig. 2. The zonal, monthly mean distribution of cloud droplet SAD (left), cloud ice SAD (middle) and total aerosol SAD (right) in April 2008. For better intercomparison of the relative magnitudes, the liquid and ice cloud SAD the values are presented here as grid-cell averages, as done for the aerosol SAD. Note the different color scale.

ACPD
14, 8575–8632, 2014

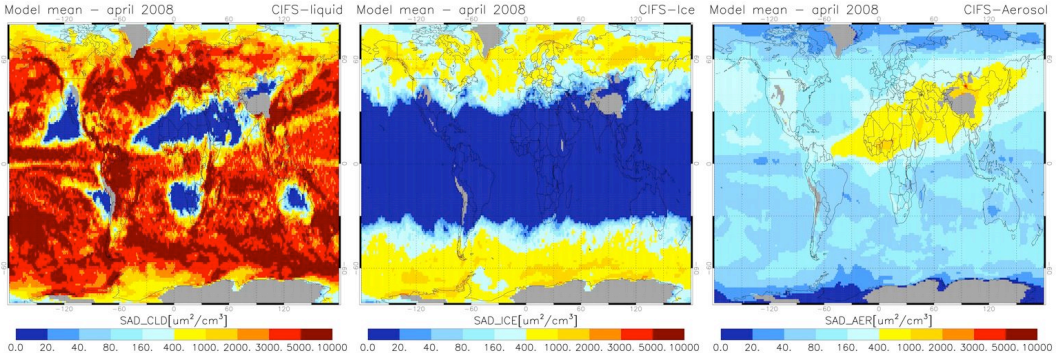

Fig. 3. Monthly mean cloud droplet SAD (left), ice (middle) and aerosol SAD (right) at 800 hPa during April 2008.

ACPD
14, 8575–8632, 2014

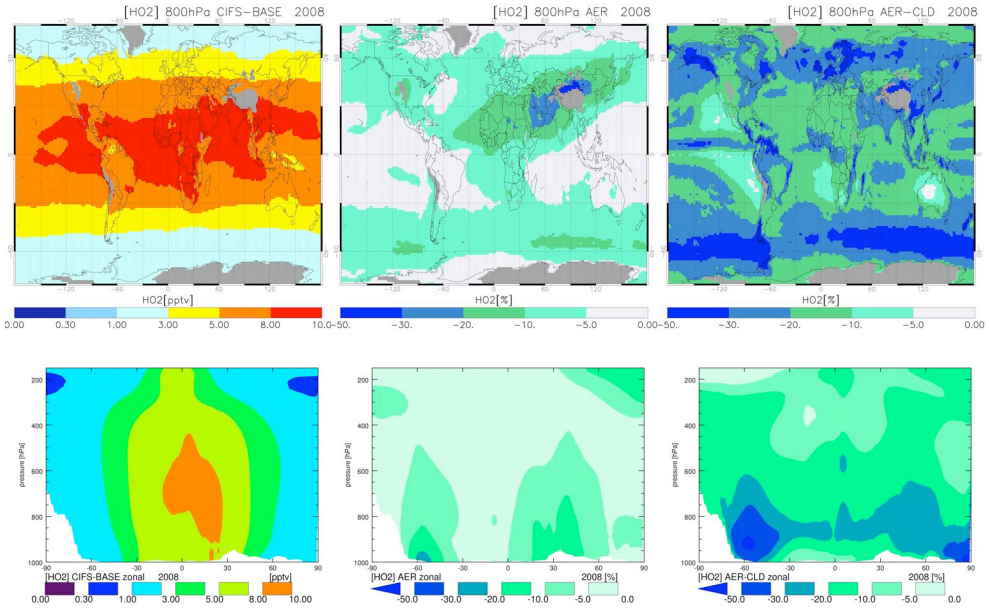

Fig. 4. The annual average distribution of global tropospheric HO_2 in 2008 for BASE (left panels) along with the relative percentual change for runs AER and AER-CLD at 800 hPa (top panels). The corresponding zonal mean distributions are shown in the lower panels.

ACPD
14, 8575–8632, 2014

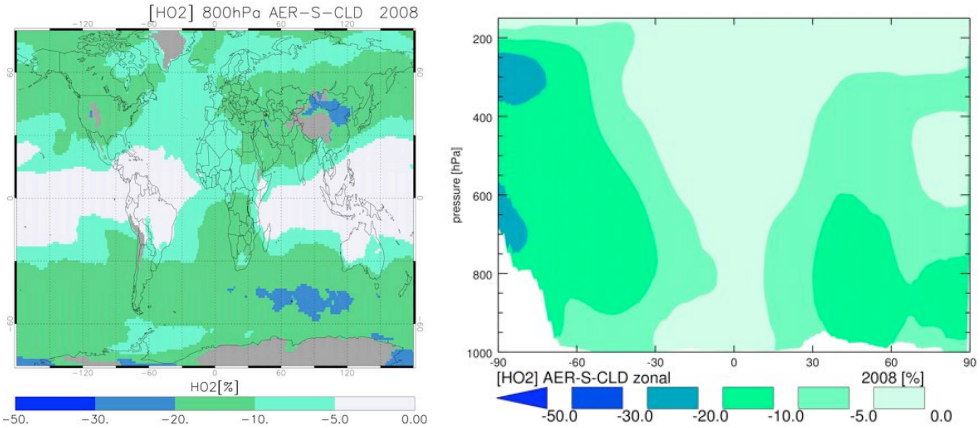

Fig. 5. The relative percentual change of global annual mean tropospheric HO_2 in 2008 for run AER-S-CLD with respect to run AER-CLD at 800 hPa (left panel) and for the zonal mean (right panel).

ACPD
14, 8575–8632, 2014

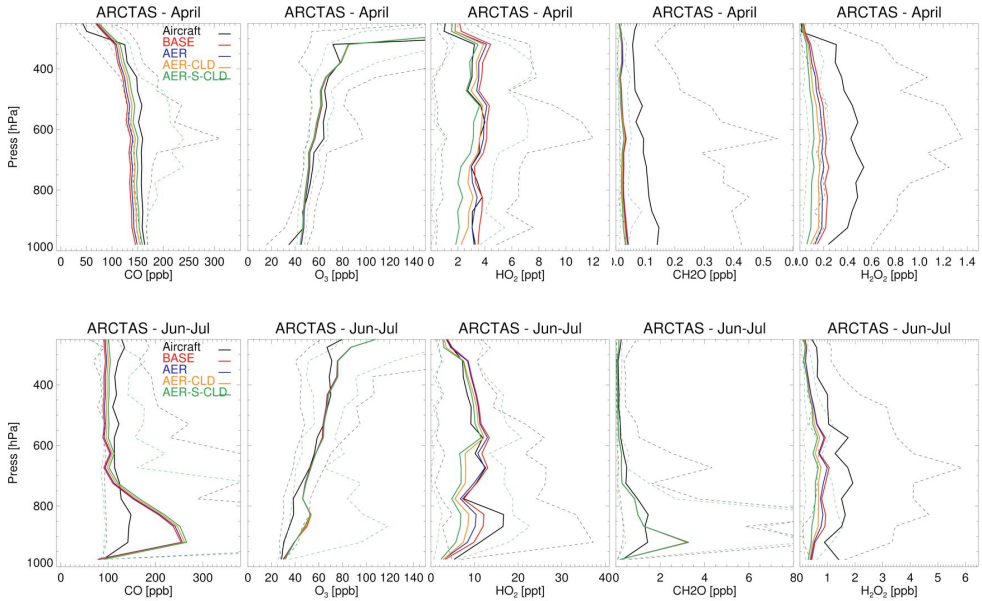

Fig. 6. Evaluation of the mean vertical tropospheric distribution of CO, O_3, HO_2, CH_2O and H_2O_2 at high northern latitudes in the C-IFS during 2008. Profiles from all model simulations are made against median ARCTAS data for April (top row) and June–July (bottom row). Dashed lines indicate the 5 and 95 percentile of the mixing ratios due to temporal and spatial variations (only shown for the observations and run AER-S-CLD).

ACPD
14, 8575–8632, 2014

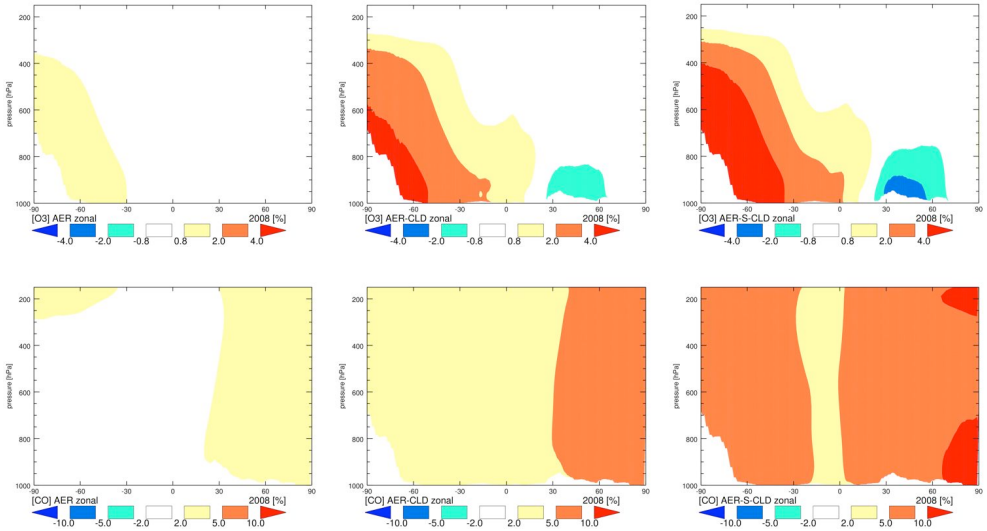

Fig. 7. The annual percentual zonal mean differences in O_3 (top) and CO (bottom) mixing ratios in 2008 for runs AER (left), AER-CLD (middle) and AER-S-CLD (right), compared to BASE.

ACPD
14, 8575–8632, 2014

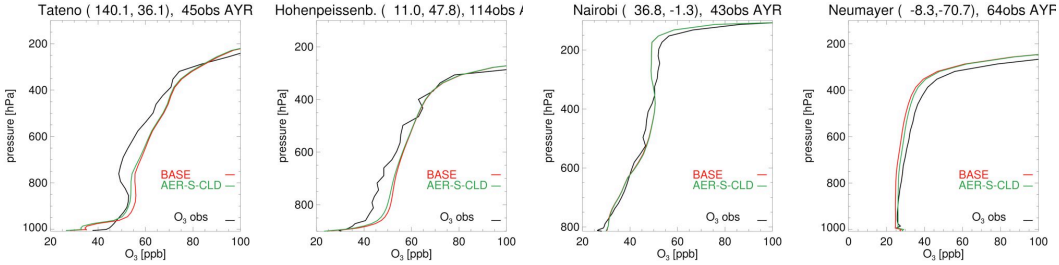

Fig. 8. Annual mean vertical profiles of tropospheric O_3 mixing ratios from C-IFS evaluated against sonde observations from (left to right) Tateno, Hohenpeissenberg, Nairobi and Neumayer. For clarity only results from BASE and AER-S-CLD are shown.

ACPD
14, 8575–8632, 2014

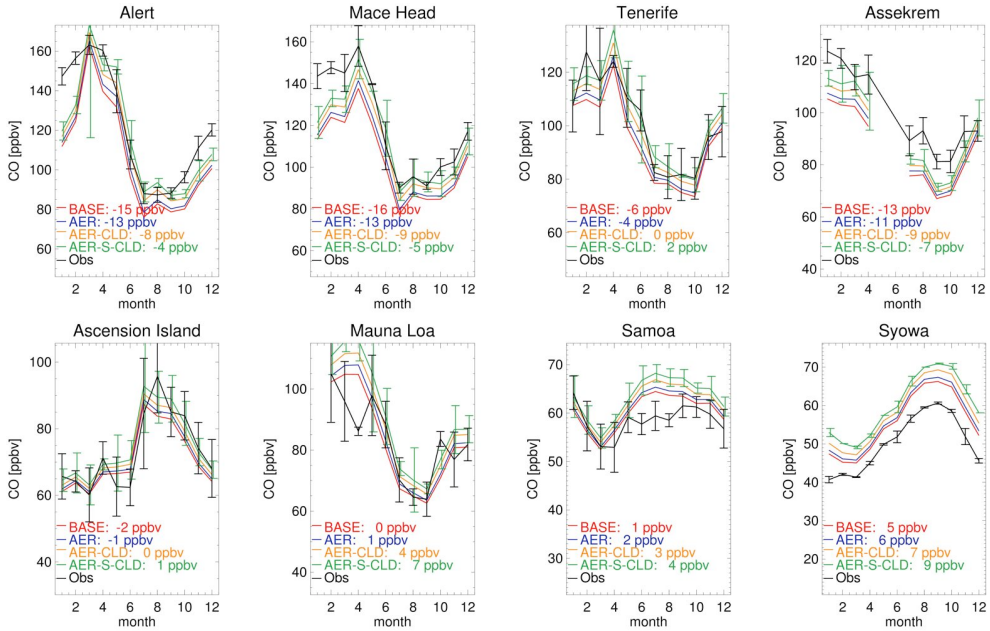

Fig. 9. An evaluation of surface CO mixing ratios in C-IFS against a selection of GMD observations. Error bars (only shown for the observations and AER-S-CLD) denote the monthly mean standard deviation in models and observations. Also given is the annual mean bias.

ACPD
14, 8575–8632, 2014

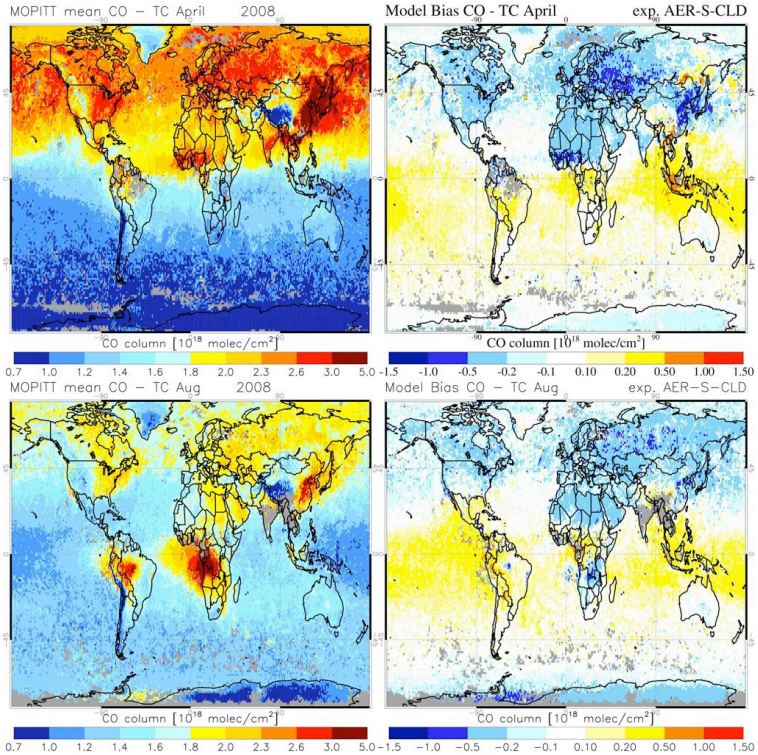

Fig. 10. Monthly mean composites of MOPITT-v6 CO total columns for April (top left) and August (bottom left) 2008. The associated bias when compared to AER-S-CLD is shown in the right panels.

ACPD
14, 8575–8632, 2014